BEHAVIOR OF MARINE SULFUR IN THE ORDOVICIAN

Linda C. Kah[1*]

Cara K. Thompson[1, 2]

Miles A. Henderson[1]

Renbin Zhan[3]

[1]Department of Earth and Planetary Sciences, University of Tennessee, Knoxville, TN 27996 USA

[2]Earth Science Department, Santa Monica College, Santa Monica, CA 90405 USA

[3]State Key Laboratory of Paleobiology and Stratigraphy, Nanjing Institute of Geology and Paleontology, Chinese Academy of Sciences, Nanjing, 210008, China

[*]Corresponding Author: lckah@utk.edu

ABSTRACT

Patterns of change in the isotope composition of sulfur-bearing minerals play a key role in reconstructing the marine sulfur cycle. Determining marine sulfate concentration, in particular, is critical to understanding the linkages between oxygenation of the Earth's atmosphere and oceans and the history of life. Much of our current understanding of marine oxygenation relies on a traditional single reservoir model, wherein the isotopic composition of marine sulfate is primarily controlled by burial of sedimentary pyrite. Utility of this model is limited, however, during times of persistent marine euxinia, which marks a fundamental decoupling between oxic and anoxic marine sulfur reservoirs. At these times, short-term fluxes that act between the two

reservoirs (e.g., sulfate reduction and sulfide oxidation processes) often dominate over the long term fluxes (e.g., weathering and pyrite burial) that control the single reservoir ocean model.

Ordovician strata from Argentina, western Newfoundland, and South China illustrate how the marine sulfur cycle is affected by the presence of a persistent euxinic reservoir. Regional euxinic reservoirs remain generally stable from the Floian through the Dapingian, despite evidence for periodic short-term oxygenation events. Dramatic reorganization of the marine sulfur cycle in the early Darriwilian, however, reflects dynamic disequilibrium between oxic and anoxic (euxinic) marine reservoirs, driven by ocean ventilation. Ventilation results in a rapid change in the isotopic composition of marine sulfate in surface oceans, and ultimately led to the near depletion of hydrogen sulfide within the anoxic reservoir, as marked by formation of superheavy pyrite. Ventilation occurs coincident with a decline in sea surface temperatures and may represent the onset of climatic change that ultimately led to late Ordovician glaciation.

Keywords: Ordovician, carbon isotopes, sulfur isotopes, euxinia

1. Introduction

Biospheric oxygen availability plays a critical role in biotic evolution because anoxia serves as a primary environmental barrier to eukaryotic life and, in particular, to the evolution of large, metabolically active animals (Knoll and Carroll 1999). The concentration of biospheric oxygen is, in turn, regulated by the geochemical cycles of carbon and sulfur (Berner et al. 2003; Canfield 2005), wherein oxygen is released via organic carbon burial and consumed by oxidation of crustal minerals, which results in pyrite oxidation and the delivery of sulfate to the oceans. Marine sulfate, with organic carbon as a reductant, is then utilized during microbial sulfate

47 reduction (MSR), producing hydrogen sulfide. This microbially produced hydrogen sulfide is
48 either reoxidized, removed from the system by reaction with reduced iron to form sedimentary
49 pyrite, or retained in the marine system as water column euxinia, where euxinia refers to anoxic
50 waters with an excess of hydrogen sulfide (HS^-). Marine euxinia may, in turn, affect biological
51 systems via availability of bioessential nutrients (Anbar and Knoll, 2002) and subsequent
52 nutrient-limitation (Van Cappellen and Ingall, 1994; Gruber and Sarmiento, 1997; Lenton and
53 Watson, 2000; Filippelli et al., 2003).
54 Marine sulfate concentration, as reconstructed via the isotopic compositions of marine
55 sulfur minerals, represents one of our most important proxies for reconstructing the history of
56 Earth oxygenation (Kah and Bartley, 2012), yet independent proxies such as iron speciation and
57 molybdenum (Raiswell and Berner, 1985; Lyons and Severmann, 2006; Canfield et al., 1992;
58 Scott and Lyons, 2005) are typically required in order to fully appreciate the complexities of the
59 marine sulfur cycle, particularly at times of persistent euxinia. Here we examine the limitations
60 of a common model used to determine marine sulfate concentration, provide high-resolution
61 carbon and sulfur isotope records from the Ordovician of Argentina, western Newfoundland, and
62 South China to illustrate how the marine sulfur cycle is affected by the presence of a persistent
63 euxinic reservoir, and examine the utility of a dual-reservoir model in better understanding the
64 behavior of the marine sulfur cycle in the Early Paleozoic.
65
66 2. Modeling sulfate reservoir size
67 *2.1. Single Reservoir Model*
68 The primary mechanism for examining the marine sulfur cycle is via a traditional isotope
69 mass balance model (cf. Kump and Arthur, 1999), wherein the ocean system contains a single

primary reservoir of marine sulfate (Fig. 1). Steady state changes in the isotopic composition of the marine sulfate reservoir are thus determined by the magnitude and isotopic composition fluxes into and out from the marine system. Input fluxes of marine sulfate include oxidative weathering of crustal sulfides (Berner, 1987) and volcanogenic sulfur species (Alt, 1995; Petsch et al., 1998), and the dissolution of sedimentary phases such as gypsum (Holser et al., 1988) and carbonate-associated sulfate (CAS; Takano, 1985; Kitano et al., 1985), although it is generally accepted, in the absence of locally enhanced volcanism, that weathering of crustal sulfides provides the primary input. Output fluxes include precipitation of CAS, marine evaporites (Raab and Spiro, 1991) and deep-sea barite deposits (Paytan et al., 2002; Torres et al., 2003), as well as the deposition of microbially mediated sedimentary sulfide minerals (Berner and Raiswell, 1983; Berner, 1984; Kump, 1989). Because precipitation of sulfate minerals and CAS results in little isotopic fractionation from the parent marine sulfate source (cf. Raab and Spiro, 1991), they are not considered to be primary drivers of the isotopic variation of marine sulfate. By contrast, bacterial sulfate reduction—with or without disproportionation reactions that characterize the oxidative parts of the sulfur cycle—can impart fractionations up to 70‰ (Harrison and Thode, 1957; Canfield and Thamdrup, 1994; Habicht and Canfield, 1996, 1997, 2001; Canfield, 2001; Canfield et al., 2010; Sim et al., 2011), and are thus considered the primary driver of isotopic change within the marine sulfate reservoir.

At steady state, fluxes into and out from the marine sulfate reservoir are equal (Fig. 1). Change in the isotopic composition of marine sulfate is defined as a time-dependent relationship, wherein changes in the isotopic composition of marine sulfate occur in response to imbalances in the fluxes into and out from a non-steady state system (Kah et al., 2004). In this case, the isotopic composition of the oceanic sulfate reservoir is defined by:

$$\partial\delta_{SO4}/\partial t = [F_W (\delta_W - \delta_{SO4}) - (F_{PY} \bullet \Delta S)] \bullet 1/M_{SO4} \quad (1)$$

wherein δ_{SO4} and δ_W are, respectively, the isotopic compositions of marine sulfate and weathering input; F_W and F_{PY} represent the magnitude of weathering and pyrite burial fluxes; ΔS represents the fractionation between oxidized and reduced sulfur reservoirs ($\Delta S = \delta_{SO4} - \delta_{py}$); and M_{SO4} represent the mass of sulfate in the marine reservoir (e.g. marine sulfate concentration).

2.2. *Limitations of single reservoir modeling*

Time-dependent relationships, along with analysis of fluid inclusions (cf. Horita et al., 2002; Brennan et al., 2004; Spear et al., 2014), have become the primary means for determining the size of the marine sulfate reservoir. Time-dependent relationships specifically highlight the effects of reservoir size on the rapidity of preserved isotopic variation, wherein small reservoir size facilitates more rapid changes in in the isotopic composition of the marine sulfate reservoir (cf. Kah et al., 2004; Hurtgen et al., 2009; Gill et al., 2011; Thompson and Kah, 2012; Luo et al., 2014a, b; Algeo et al., 2015). Yet, despite the success of this time-dependent approach, it has very specific limitations when it comes to interpreting the evolution of the marine sulfur cycle.

The time-dependent model developed by Kah et al. (2004), for instance, assumes that observed trends on the isotopic composition of CAS reflect only a portion of the maximum possible rate of isotopic change, where the maximum rate of isotopic change is defined by the residence time of sulfate in the oceans. Sulfur isotope trends for late Palaeozoic and younger strata (Burdett et al., 1989; Strauss et al., 1997; Paytan et al., 1998) suggest that, when oceans are well mixed, rates of marine isotopic change reflect only 3–14% of maximum possible rates of

116 isotopic change. Times of local to regional anoxia, such as during the Cretaceous anoxic events,
117 record much more rapid rates of isotopic change (Okouchi et al., 1999; Owens et al. 2013).
118 Although this assumption is necessary for the purposes of the model, it must be kept in mind that
119 if observed rates of isotopic change are less than the assumed proportion of maximum possible
120 rates of change, then the model will overestimate the size of the marine sulfate reservoir.
121 Variation in the degree to which observed rates of isotopic change reflect the theoretical
122 maximum for a given marine sulfate concentration also depend on natural variation in the
123 isotopic composition and rate of weathering and pyrite burial. Although the time-dependent
124 model is not particularly sensitive to changes in F_W, it is substantially more sensitive to F_{PY} and
125 ΔS (Kah et al., 2004). To better constrain seawater sulfate concentration, Algeo et al (2014)
126 developed a variation of this time-dependent model wherein additional constraints are placed on
127 F_{PY} via expectations of steady state weathering fluxes in a low-oxygen world, and on ΔS via
128 observational and experimental work that relates sulfate concentration to the isotope composition
129 of hydrogen sulfide resulting from bacterial sulfate reduction (Detmers et al., 2001; Brüchert,
130 2004; Gomes and Hurtgen, 2013, 2015).
131 Perhaps more importantly, a single-reservoir model assumes that the vast majority of
132 hydrogen sulfide resulting from MSR is immediately reoxidized (e.g., in the modern ocean, as
133 much as 95% of hydrogen sulfide generated by MSR is reoxidized to sulfate and intermediate S
134 species; Jorgensen et al., 1990). Under low oxygen and low sulfate conditions that characterized
135 much of the Earth's ancient past, the percentage of hydrogen sulfide reoxidized may have been
136 substantially lower. In this case, behavior of the sulfate reservoir will be strongly dependent on
137 the availability of reduced iron in the marine system. If reduced iron is available to strip the
138 water column of microbially produced hydrogen sulfide, burial of sedimentary pyrite will be

maintained (Hurtgen et al., 2005) given sufficient marine sulfate. If, however, marine sulfate concentrations were exceedingly low (e.g., as is estimated for some Paleoproterozoic units; Luo et al., 2014b; Guo et al., 2015), pyrite burial fluxes could be reduced to a degree that restricts the potential for isotopic change in the overall reservoir. Similarly, if reduced iron availability is insufficient to strip the water column of microbially produced hydrogen sulfide, euxinic conditions will develop. Euxinic waters would thus represent a reduced sulfur reservoir that is distinct from the traditional marine sulfate reservoir.

3. Marine sulfur in the Early to Middle Ordovician

Our current understanding of sulfur cycling in the Ordovician is primarily rooted within studies of earlier Paleozoic geochemical change. High-resolution sulfur isotope data from Cambrian (Goldberg et al., 2005; Hough et al., 2006; Hurtgen et al., 2009: Gill et al., 2011; Wotte et al., 2012) successions show rapid fluctuation in the isotopic composition of CAS and variability in composition between disparate stratigraphic successions. Together, these suggest non-conservative behavior of marine sulfate and support inferences of low marine sulfate. Combined, single-reservoir time-dependent models (Hurtgen et al., 2009: Gill et al., 2011) and extrapolation from fluid inclusions (Horita et al., 2002; Brennan et al., 2004) suggest sulfate concentrations <2-12 mM. In addition to low marine sulfate, indications of at least local euxinic conditions in geographically disparate Cambrian successions (Goldberg et al., 2005; Wille et al., 2008; Hurtgen et al., 2009; Gill et al., 2011; Feng et al., 2014) suggest that conditions for euxinia may have been widespread in the early Paleozoic. Evidence for sulfidic (Hammarlund et al., 2012; Zhou et al., 2015), potentially sulfidic (Zhang et al., 2011; Hints et al., 2014), and ferruginous water bodies in the late Ordovician (Yan et al., 2012), as well as inferences from

both C-isotopes (Saltzman, 2005) and CAS behavior (Thompson and Kah, 2012; Marenco et al., 2013) for persistent euxinia in platform environments of the middle Ordovician, suggest that euxinic conditions likely occurred as regional, mid-depth (i.e. beneath an oxidized surface layer) water bodies, close to inferred continental margins. Combined, these datasets suggest that current single-reservoir models do not necessarily provide a comprehensive view of the marine sulfur cycle in the Early Paleozoic.

3.1. Geological sections

At the onset of the Ordovician, the paleogeographic positions of the major paleocontinents are fairly well constrained (Cocks and Torsvik, 2002, 2011; Torsvik and Cocks, 2009, 2013) (Fig. 2). Gondwana, consisting of present-day South America, Africa, India, Australia, Antarctica, and Arabia, spanned from mid-northerly latitudes to the South Pole. Laurentia and Siberia both occurred in equatorial positions, and Baltica occupied a position in mid-southerly latitudes. Numerous other microcontinents and continental fragments were positioned around Gondwana, such as the Avalon peri-Gondwanan terrane (Harper et al., 1996; MacNiociall et al., 1997), or further afield, the North and South China cratons and Tarim microcontinent (Cocks and Torsvik, 2013).

The Ordovician was marked by dramatic changes in plate tectonic configuration, including the northward dispersal of peri-Gondwanan terranes, such as the South China craton (Chen et al., 2004), and the evolution of the Iapetus and Rheic oceans (Murphy et al., 2010; Nance et al., 2012; Van Staal et al., 2012). Foundering of Iapetus and expansion of the Rheic ocean, in particular, was associated with both the migration of the Avalon terrain from its peri-Gondwana position to its eventual docking on Laurentia (Keppie and Keppie, 2014) and the rifting of the

185 Precordilleran microcontinent from the southeast margin of Laurentia to its subsequent docking
186 with Gondwana (Thomas and Astini, 1996, 1999). Rapid changes in plate-tectonic configuration
187 in the Ordovician ultimately led to globally high sea level (Miller et al., 2005; Haq and Shutter,
188 2008), flooding of the continental shelves (Algeo and Seslavinsky, 1995), and widespread
189 development of epeiric seas.
190 Marine carbonate rocks of the Ordovician have long been the focus of paleontological
191 studies examining marine diversity, ecology, and biogeography (e.g., Harper et al., 1996; Miller,
192 1997; Droser and Finnegan, 2003; Servais et al., 2008, 2010; Rasmussen and Harper, 2008;
193 Buatois et al., 2009). Addition of stratigraphically constrained geochemical analysis of carbon
194 (Saltzman and Young, 2005; Young et al., 2005, 2008; Schmitz and Bergstrom, 2007; Bergstrom
195 et al., 2008; Ainsaar et al., 2010; Zhang et al., 2010; Munnecke et al., 2011; Thompson et al.,
196 2012; Albanesi et al., 2013; Sial et al., 2013; Edwards and Saltzman, 2014) and strontium (Qing
197 et al., 1998; Shields et al., 2003; Young et al., 2009; Hannigan et al., 2010) isotopes have
198 provided critical insight into the global correlation of these units. Here we examine the marine
199 sulfur isotope record of marine carbonate rocks of the Argentine Precordillera, western
200 Newfoundland, and the Yangtze platform of South China as an example of how sulfur isotopes
201 can provide insight into marine dynamics of the Ordovician.
202
203 *3.1.1. Argentina*
204 Lower Paleozoic strata of the Argentine Precordillera comprise >2500 meters of mixed
205 carbonate, siliciclastic, and evaporite units that were deposited in a range of supratidal to deep
206 subtidal environments (Astini et al., 1995). Basal strata of the Cambrian Cerro Totora, La Laja,
207 Zonda, and LaFlecha formations (Thomas and Astini, 2003; Gomez et al., 2007) mark rifting of

208 the Precordilleran terrane from southern Laurentia and development of a long-lived passive
209 margin. Passive margin deposition continued from the Cambrian through the Early Ordovician,
210 with peritidal marine deposition of the LaSilla Formation (Cañas, 1999; Thompson and Kah,
211 2012). Conformably overlying strata of the Lower to Middle Ordovician San Juan Formation
212 record the development of deeper water carbonate environments with convergence of the
213 Precordillera terrain toward the Gondwanan Famatina terrain (Astini et al., 2007). Convergence
214 of the Precordillera terrane with Gondwana is marked by the widespread appearance of
215 Dapingian to Darriwilian (464 to 473 Ma; Huff et al., 1997; Fanning et al., 2004; Thompson et
216 al., 2012) K-bentonites and a north–south diachronous development of deep-water shale, mixed
217 carbonate-shale, and carbonate of the Gualcamayo, Las Chacritas, and Las Aguaditas formations.
218 This study focuses on the carbonate-dominated strata of the San Juan, Las Chacritas, and
219 Las Aguaditas formations (Figs. 3A, 4). Samples were collected every 6 to 9 meters from
220 multiple measured stratigraphic sections of the San Juan Formation, as well as single measured
221 sections of the Las Chacritas and Las Aguaditas formations at Las Chacritas Creek and Las
222 Aguaditas Creek, respectively, where these units conformably overlie strata of the San Juan
223 Formation. The San Juan Formation consists of nearly 450 meters of heterogeneous shallow
224 subtidal carbonate platform deposits. Deepest-water facies include fossiliferous wackestone and
225 nodular mudstone, as well as storm-dominated bioclastic limestone. Shallow-water facies, which
226 occur primarily in the lower San Juan Formation include oolitic and oncolitic packstone and
227 discrete bioherms consisting of microbial- and sponge-dominated calcareous boundstone (Cañas
228 and Carrera, 1993). The top of the San Juan Formation is time-transgressive (Astini, 1995;
229 Thompson et al., 2012) and is conformably overlain with interbedded bioclastic wackestone and
230 shale of the Las Chacritas (100 meters measured at Las Chacritas Creek) and the Las Aguaditas

231 (330 meters measured at Las Aguaditas Creek) formations, or calcareous to black shale of the
232 Gualcamayo Formation (Thompson et al., 2012).
233
234 *3.1.2. Western Newfoundland*
235 More than 2500 meters of early Paleozoic strata are exposed in the Humber Zone of
236 Western Newfoundland (Fig. 3B) and record the development and eventual foundering of a long-
237 lived, Laurentian passive margin (Stenzel and James, 1987; James et al., 1989; Lavoie et al.,
238 2003). In western Newfoundland, post-rift strata of the early Cambrian are represented by
239 siliciclastic rocks of the Labrador Group (Bradoew, Forteau, and Hawkes Bay formations).
240 Passive margin development in the late Cambrian is marked by deposition of carbonate-
241 dominated, high-energy strata of the Port-au-Port Group (March Point, Petit Jardin, and Berry
242 Head formations). Passive margin deposition continued through the early and middle Ordovician
243 with carbonate-dominated, low-energy deposition of the St. George Group (Watts Bight, Boat
244 Harbour, Catoche, and Aguathuna formations) (James et al., 1989). By the earliest Dapingian,
245 subduction associated with the approach of the peri-Gondwanan Avalon terrane resulted in short-
246 lived erosion of the uppermost St. George Group followed by renewed subsidence and eventual
247 foundering of the carbonate platform, recorded in deposition of the Dapingian to Dariwilian-aged
248 Table Head Group (Table Point, Table Cove, and Black Cove formations) (James et al., 1989;
249 Stenzel et al., 1990).
250 This study focuses on the latest Floian to mid-Darriwilian strata of the Aguathuna, Table
251 Point, and Table Cove formations (Fig 4). Samples were collected every 9 meters from a
252 measured section at Table Point, western Newfoundland. Nearly 75 meters of the Aguathuna
253 Formation were sampled at Table Point, where strata consist primarily of mottled lime mudstone,
254 fossiliferous packstone, and oolitic and intraclastic grainstone. Upper portions of the Aguathuna

255 are associated with abundant secondary dolomitic veins, and substantially overprinted with
256 sucrosic dolomite. The boundary between the Aguathuna Formation and overlying Table Head
257 Group is marked by an abrupt change from coarsely recrystalline, buff-colored dolomite to a
258 >250 meter thick, monotonous section composed of predominantly dark grey lime mudstone and
259 fossiliferous wackestone, with subordinate fossiliferous packstone, minor peloidal grainstone,
260 and conspicuous intervals containing small sponge bioherms (cf. Klappa et al., 1980). Only the
261 lowermost 50 meters of the overlying Table Cove Formation were sampled at Table Point. Table
262 Cove strata consist of intercalated limestone and shale with distinct intervals of slumping that
263 transition upward into predominantly black shale lithologies of the upper Table Cove and
264 overlying Black Cove formations.
265
266 *3.1.3. China*
267 The South China craton is divided into three primary regions: the Yangtze platform, the
268 Jiangnam slope, and the Zhujiang basin (Chen et al., 2004) that represent nearly complete
269 flooding of the craton during the Ordovician (Fig. 3C). The Yangtze platform, in particular, is
270 characterized by a broad, pericratonic marine platform and preserves a nearly complete
271 stratigraphic succession through the Ordovician. This stratigraphic succession can be up to 500
272 meters thick and consists of the carbonate dominated Xilingxia, Nantsinkuan, Fengshiang,
273 Hunghhuayuan, Dawan, Kuniutan, and Pagoda formations, and the siliciclastic dominated
274 Miaopo Formation—which separates the underlying Kuniutan and Pagoda formations—and the
275 upper Linhsiang, Wufeng, and Kuanyinchia formations.
276 This study focuses on the carbonate-dominated Hunghhuayuan, Dawan, and Kuniutan
277 (*alternately* Guniutan) formations as exposed in the Chenjiahe section, just north of Yichang in

278 the north-central Yangtze platform (Fig. 4). Samples were collected at intervals of 3 to 6 meters
279 from a measured stratigraphic section, and positions in the stratigraphic section were linked to
280 previously determined biostratigraphic boundaries (Zhan and Jin, 2007). At Chenjaihe, the
281 Hunghhuayuan formation is approximately 24 meters thick and is similar in its facies to
282 elsewhere on the Yangtze platform, consisting of medium to thick-bedded, variously bioclastic
283 limestone, with minor biohermal limestone. Bioclastic limestone is characterized as sparse to
284 packed biomicrite containing abundant crinoids, trilobites, and brachiopods, with minor
285 bryozoans. At several horizons, small bioherms composed of convex-upward calcareous sponges
286 record *in situ* carbonate production.
287 Conformably overlying the Hunghuayuan is the Dawan Formation. The Dawan Formation
288 represents a highly condensed equivalent to the Meitan Formation, which occupies the majority
289 of the Yangtze platform (cf. Munnecke et al., 2010; Zhang et al., 2010). At Chenjaihe, the
290 Dawan Formation is approximately 45 meters thick and consists predominantly of thin,
291 interbedded argillaceous limestone, nodular limestone, calcareous mudstone, and black shale.
292 The central portion of the Dawan formation contains conspicuous purple micrite that is
293 interpreted to represent maximum flooding and stratigraphic condensation of the Yangtze
294 platform. Stratigraphic condensation is a hallmark of the Dawan Formation, which is
295 substantially thinner than the >250 m thick time-equivalent sections of the Meitan Formation (cf.
296 Zhang et al., 2010). The conformably overlying Kuniutan Formation marks a return to more
297 carbonate-rich deposition. At Chenjiahe, the Kuniutan Formation consists of approximately 30
298 meters of monotonous, medium bedded, nodular to argillaceous, bioclastic limestone.
299
300 *3.2. Geochemical Methods*

301 *3.2.2. Petrographic screening*

302 Prior to isotopic and elemental analyses, samples were evaluated using standard
303 petrographic and cathodoluminescence (CL) techniques (Kah et al., 1999; Frank et al., 2003;
304 Bartley et al., 2007; Kah et al., 2012) to identify the preserved range of depositional and
305 diagenetic carbonate fabrics. Approximately 2 mg of powdered sample was collected from
306 homogeneous phases within polished thick sections using 0.25 and 0.50 mm drill bits mounted
307 on a Servo micro-drill press. Where possible, multiple carbonate phases were sampled in order to
308 provide a first-order assessment of depositional and diagenetic heterogeneity via elemental (Ca,
309 Mg, Sr, Mn, Fe) and isotopic (C, O) analysis. Samples showing evidence of substantial
310 secondary recrystallization were not used for bulk-rock analyses.

311

312 *3.2.3. C- and O-isotope analyses*

313 Micro-drilled carbonate phases were analyzed for C- and O-isotope composition for
314 evaluation of potential diagenetic alteration and to establish chemostratigraphic correlations of
315 Ordovician strata. Approximately 0.5 to 1.0 mg of powder from micro-drilled carbonate phases
316 was loaded into silver capsules, reacted with anhydrous phosphoric acid at 120 °C, and
317 cryogenically distilled using a Carbo-Flo automated sampler attached to a duel inlet Finnigin
318 MAT Delta Plus gas source isotope ratio mass spectrometer at the University of Tennessee. Data
319 are reported in delta notation as per mil (‰) deviations from Vienna Pee Dee Belemnite (VPDB).
320 Analyses were determined to be reproducible to within ±0.1‰ from analysis of duplicate and
321 internal lab standards.

322

323 *3.2.4. Major and trace element analyses*

Micro-drilled carbonate phases were analyzed for major and trace element concentrations for evaluation of potential diagenetic alteration. Approximately 1 mg of micro-drilled powder was dissolved, with agitation, in 10 ml of trace metal grade 2% HNO_3. Samples were then centrifuged for 10-15 min at 3000 rpm to separate and pelletize insoluble residue; the top 9 ml of solution was then decanted to a clean centrifuge tube. Elemental analyses were conducted at the University of West Georgia using a Perkin-Elmer inductively coupled plasma optical emission spectrometer (ICP-OES) fitted with a Meinhardt concentric nebulizer, or at the University of Tennessee using a Perkin-Elmer Optima 2100 DV ICP-OES with a Scott spray chamber. All analyses were calibrated using a series of gravimetric standards that were run before and after every six unknowns. Analyses were determined to be reproducible to within ±10% by analysis of standards and duplicate samples.

3.2.5. Sulfur extraction and isotope analyses

Carbonate-associated sulfate (CAS) was extracted from carbonate lithologies in order to understand time-wise changes in marine sulfate composition. CAS substitutes into the carbonate lattice during carbonate precipitation and is often regarded as a reliable proxy for marine sulfate composition on both modern and ancient samples (Burdett et al., 1989; Strauss, 1997, 1999; Kampschulte et al., 2001; Kah et al., 2004). Although complexity of interpretation can arise from possible vital effects and the potential of mixed sources of sulfate during deposition and sea-floor stabilization (Present et al., 2015), limited studies suggest that CAS may be resistant to changes in isotopic composition during later diagenesis, despite reduction in sulfate concentration during recrystallization (Lyons, 2004; Gill et al., 2008; Rennie and Turchyn, 2014).

CAS was extracted using methods modified from Burdett et al. (1989), Hurtgen et al.

(2002), and Kah et al. (2004). Bulk rock sections were etched with 10% HCl to remove surface weathering products, crushed to 1-3 mm diameter chips, picked to avoid secondary phases, then powdered. Approximately 50-100 g of powdered sample was soaked overnight in 250 ml of 5.65–6% sodium hypochlorite (NaOCl), to remove soluble iron sulfide and organically bound sulfur, rinsed with Milli-Q water, and filtered. Dried samples were dissolved slowly with up to 600 mL of 3 N hydrochloric acid. Dissolution was monitored to maintain a pH>3 to prevent the exchange of oxygen between sulfate and water and to minimize pyrite oxidation (Chiba and Sakai, 1985). Samples were filtered to remove insoluble and undissolved residue, and the filtrate was brought to a pH of 9 using sodium hydroxide (NaOH) pellets to precipitate dissolved iron oxide. After filtering any precipitate phases, approximately 150 mL of saturated barium chloride solution (250 g/L) was added to the filtrate to recover CAS as barium sulfate. The reaction was allowed to continue overnight at room temperature to ensure complete precipitation of CAS as barium sulfate.

Pyrite sulfur was extracted by sequential acid extraction (Canfield et al., 1986). Elemental and organically-bound sulfur were extracted by rinsing 5 grams of sample with approximately 250 ml of heated dichloromethane for 12-18 hours. Elemental sulfur was collected on copper pellets during dichloromethane digestion and later collected using silver nitrate traps; negligible elemental sulfur was obtained from samples. Sulfate and monosulfides were then extracted by dissolution of the dried powders in 6N hydrochloric acid under a nitrogen atmosphere. Acid-volatile monosulfides were collected in silver nitrate traps, filtered and weighed. Iron oxide was removed from the filtrate by increasing the pH to 9, leaving overnight and filtering. The pH of the filtrate was lowered to 4 using HCl, and barium sulfate precipitated by adding 10 ml of 10% barium chloride. Samples that yielded sufficient $BaSO_4$ were analyzed for isotopic composition

as replicates of bulk rock CAS extractions, and were found, within error, to reproduce the isotopic composition of larger bulk samples. The remaining sample was dissolved in a 1:1 12N hydrochloric acid and chromium chloride solution under a nitrogen atmosphere for pyrite extraction. Pyrite-sulfur was collected in silver nitrate traps, filtered and dried overnight prior to weighing and isotopic analysis. Samples were analyzed for $\delta^{34}S$ using a Finnigan MAT 252 gas source mass spectrometer fitted with an elemental analyzer at Indiana University. S-isotope composition is expressed as per mil (‰) deviation from Vienna Canyon Diablo Troilite (VCDT). Analytical precision was determined to be ±1‰ by analysis of lab standards.

3.3. Results

Geochemical results are summarized in Table 1. Data from the San Juan Formation can be found in Thompson and Kah (2012). Data for all other formations is detailed in Tables 1–3 *(supplementary information)*, and presented in Figures 6–10.

3.3.1. Potential for diagenetic overprinting

Multiple lines of evidence were used to evaluate the degree to which geochemical measurements represent syndepositional marine signatures (cf. Frank and Lohmann, 1996; Kah et al., 1999, 2012; Bartley et al., 2007). Petrographic analyses reveal that, in all sections, the primary lithology is variably fossiliferous wackestone. Skeletal material consists largely of bryozoan and echinoderm fragments that comprise 20-30% of the rock; matrix components consist of micrite and finely crystalline microsparite (Fig. 5). Skeletal fabrics are typically well-preserved and show little evidence for diagenetic recrystallization except for rare aragonitic fossil phases (e.g. molluscs). Packstone and grainstone lithologies are less common and occur

393 primarily in peritidal facies of both Argentina (San Juan Formation; *see* Thompson and Kah,
394 2012) and China (Huanhuayuang Formation). Peritidal facies show clear preservation of both
395 marine and fresh-water precipitates as both grain coatings of isopachous cement and as equant
396 spar within peritidal fenestrae, as well as detailed preservation of primary grains (e.g., radial
397 ooids, *Girvanella*). Strongly fenestral fabrics were easily recognized in crushed sample, and
398 avoided during powdering. Deeper subtidal facies of Argentina (Las Aguaditas Formations) and
399 China (Dawan Formation) are lithologically homogeneous, consist primarily of organic-rich
400 laminated micrite, with a generally 10-20% fossiliferous component. Deeper water facies show
401 little evidence for the presence of secondary diagenetic phases. Late-diagenetic phases occur
402 primarily as mineralized fractures, although only some of these (Aguathuna Formation) are
403 associated with substantial recrystallization of host rock.
404 The extent of post-depositional water-rock interaction can also be evaluated by comparing
405 preserved trends in both oxygen isotope and trace element composition. Oxygen isotopes of
406 primary depositional phases fall between –4.5 and –7.5‰ (Table 1). Because oxygen isotopes
407 are readily exchanged during water-rock interaction (Banner and Hanson, 1990), Paleozoic rocks
408 that contain depositional phases with little petrographic evidence for recrystallization and oxygen
409 isotope values more positive than –8‰ are generally considered to have undergone minimal
410 post-depositional alteration (Wadleigh and Veizer, 1992; Qing and Veizer, 1994; Veizer et al.,
411 1999). An interpretation of minimal diagenetic recrystallization under high water-rock ratios is
412 consistent with the presence of vein-filling material in each succession that records substantially
413 different oxygen isotope compositions than surrounding host rock (*see also* Azmy et al., 2008).
414 Trace element composition provides an additional indication of post-depositional
415 diagenesis. The majority of rocks in these successions are calcitic, with Mg/Ca ratios near 0 ppm,

416 with only minor evidence for post-depositional dolomitization. Strontium concentrations fall
417 primarily between 200 and 1200 ppm, which is within the range of marine calcite that has
418 undergone only limited Sr-loss associated with post-depositional recrystallization (Banner and
419 Hanson, 1990). Notably, the lowest Sr concentrations occur within the Aguathuna Formation,
420 which is consistent with Sr loss during post-depositional fluid flow and dolomitization. By
421 contrast, manganese concentration, which is often used as an indicator of recrystallization during
422 burial diagenesis, is more variable. Manganese concentrations in both Argentina and
423 Newfoundland fall predominantly below 400 ppm, resulting in Mn/Sr ratios typically less than
424 the empirical thresholds derived for "little altered" carbonate lithologies (Derry et al., 1992;
425 Kaufman and Knoll, 1995), yet greater than that suggested for "pristine" carbonate lithologies
426 (Montanez et al., 1996). Samples from South China, however, preserve substantially elevated
427 Mn concentrations, with samples from the Hunghuayuan Formation averaging 698 ppm, and
428 samples from the overlying Dawan and Kuniutan formations averaging 2985 and 862 ppm,
429 respectively. These elevated Mn concentrations are interesting in that they occur in rocks with
430 both elevated Sr concentrations and oxygen isotope compositions indicative of only minor post-
431 depositional recrystallization. Additionally, Mn concentrations appear to coincide with
432 depositional facies, with deepest-water facies of the Dawan Formation substantially enriched in
433 Mn. Carbonate within these strata are distinctly purple, and correlate offshore to sedimentary Mn
434 deposits of the Zhujiang slope, suggesting that elevated Mn is related to marine transgression and
435 interaction with low oxygen fluids (cf. Kah et al., 2012; Gilleaudeau and Kah, 2013) that
436 facilitate Mn reduction and deposition in marine sediments (Davison, 1982). A large range in Mn
437 concentration is also preserved within the Aguathuna Formation. In this case, elevated Mn is
438 associated with low Sr concentration and petrographic evidence for replacive dolomite formation,

suggesting interaction with burial fluids (cf. Azmy et al., 2008).

3.3.2. Marine carbon isotope compositions

Petrographic and geochemical indicators suggest that Ordovician carbonate strata from Argentina, Newfoundland, and South China underwent only minimal post-depositional recrystallization and likely preserve marine isotopic compositions. Carbon isotope compositions from all sections are similar, ranging between –2 and +1‰ (Table 1), and show markedly coherent stratigraphic patterns (Fig. 6). Carbon isotopes from the Argentine Precordillera (*see also* Thompson and Kah, 2012; Thompson et al., 2012) record a sharp excursion to -2.5‰ in the early Floian (basal San Juan Formation), followed by a broad positive feature wherein isotopic values return to near 0‰ in the mid-Floian before gradually falling to –1‰ in the early Dapingian. The middle Dapingian (Upper San Juan Formation) is marked by a second short, yet distinctive negative excursion to values near –2‰. Both the early Floian and middle Dapingian excursions have been recognized globally (Buggisch et al., 2003; Männik and Viira, 2005; Bergstrom et al., 2008; Azmy and Lavoie, 2009; Edwards and Saltzman, 2014), and recent U-Pb dating of zircon within bentonite deposits in the Argentina sections have constrained the peak of the middle Dapingian excursion to between 469.86 ±0.62 and 469.60 ±0.60 (Thompson et al., 2012). Carbon-isotope values then return to approximately –0.5‰ by the start of the Darriwilian, followed by an abrupt rise to values near +1‰ in the middle Darriwilian (Las Chacritas and Las Aguaditas formations), representing the globally recognized MDICE excursion (Ainsaar et al., 2004, 2010; Kaljo et al., 2007; Bergstrom et al., 2008; Schmitz et al., 2010).

Although sampled strata in Newfoundland and South China record shorter intervals within the Ordovician, biostratigraphic data permits detailed carbon isotopic correlation. In western

462 Newfoundland, the uppermost Aguathuna Formation is identified to occur within the Orthidella
463 brachiopod zone (early Dapingian; Williams et al., 1987), suggesting that the Floian-Dapingian
464 boundary lies near the top of the formation. The overlying Table Head Group contains conodonts
465 that extend to the *P. anserinus* zone, indicating deposition spanning from the Dapingian through
466 the Darriwilian (Williams et al., 1987). Only the lowermost portion of the Table Cove Formation
467 was sampled for this study, however, suggesting termination of the chemostratigraphic profile
468 prior to the late Darriwilian. The carbon-isotope profile for Newfoundland is consistent with
469 deposition from the late Floian (uppermost Aguathuna Formation) through the middle
470 Darriwilian (basal Table Cove Formation) (Fig. 6). Carbon-isotope values near –1‰ drop rapidly
471 in the lower Table Point Formation to values near –2‰, followed by a return to values near –
472 0.5‰ and a sharp rise to values near +1‰ in the lowermost Table Cove Formation. This pattern
473 is interpreted to reflect the middle Dapingian negative excursion, recovery, and entry into the
474 positive MDICE excursion (Thompson et al., 2012). Absence of a positive isotopic plateau, as
475 recorded in the Argentine section, suggests that strata of the basal Table Cove Formation lie
476 within the middle Darriwilian.

477 Biostratigraphic details of the Ordovician of the Yangtze platform have been studied
478 extensively (Chen et al., 1995; Zhang and Chen, 2003; Zhan et al., 2007; Zhan and Jin, 2008).
479 The lowermost Hunghuayuan Formation is defined by conodonts of the *P. elongates-deltifer* and
480 *P. elegans* zones, indicating a lower Floian age for deposition. The conformably overlying
481 Dawan Formation spans from the *D. eobifidus* to *U. astrodentatus* graptolite zones, or from the
482 upper Floian to lower Darriwilian. The overlying Kuniutan Formation is constrained by both
483 graptolites and conodonts to have been deposited wholly within the Darriwilian. With these
484 constraints, detailed chemostratigraphic correlation is possible (Fig. 6). The Hunghuayuan

485 Formation records carbon isotope values near –1.5‰. These are the lightest isotopic
486 compositions of the succession and are consistent with the early Floian negative excursion. In the
487 overlying Dawan Formation, carbon isotope values rise to values of approximately +0.5‰ before
488 rapidly falling to –1‰. This sharp negative excursion, here interpreted as the middle Dapingian
489 negative excursion, is followed by recovery to carbon isotope values near 0‰ in the uppermost
490 Dawan Formation and continuation of this rise through the Kuniutan Formation to values near
491 +1‰. Rise to values near +1‰ in the Kuniutan are consistent with entry into the positive
492 MDICE excursion, and is consistent with interpretations of the carbon isotope record elsewhere
493 in the Yangtze platform (Munnecke et al., 2010; Schmitz et al., 2010; Zhang et al., 2010).
494
495 *3.3.3. Marine sulfur isotope compositions*
496 In light of minimal evidence for post-depositional recrystallization and markedly coherent
497 carbon isotope chemostratigraphy, we expect similarly well-preserved isotopic records for
498 marine sulfur. The sulfur isotope composition of marine waters was determined via carbonate-
499 associated sulfate (CAS). CAS substitutes into the carbonate lattice during carbonate
500 precipitation and is broadly regarded as a reliable proxy for marine sulfate (Burdett et al., 1989;
501 Strauss, 1999; Kampshulte et al., 2001).
502 Until recently, CAS has been considered remarkably resistant to post-depositional isotopic
503 exchange (Lyons et al., 2004). Despite evidence for up to 80% loss of CAS during diagenetic
504 recrystallization (Gill et al., 2008), the isotopic composition of CAS has been shown, in any but
505 the most pyrite-rich samples (cf. Mazmudar et al., 2008; Marenco et al., 2008), to vary little
506 during recrystallization. Recent analyses by Present et al. (2015), however, suggest potential for
507 CAS to reflect a more complex story of deposition and diagenesis. By utilizing new technologies

508 that permit extraction and isotopic analysis of CAS from individual carbonate phases, Present et
509 al. (2015) showed wide variation in the isotopic composition of CAS from within single geologic
510 samples. Using petrographically well-preserved brachiopod calcite as a marker for seawater
511 composition, they showed that trilobites, echinoderms, and bryozoans preserve S-isotope values
512 that are enriched in ^{34}S by up to 5‰. By contrast, fine-grained matrix components recorded S-
513 isotope values that ranged from inferred seawater composition to isotope values depleted in ^{34}S
514 by up to 15‰. Present et al. (2015) suggest that variation in CAS composition within a
515 succession may thus reflect a combination of differences in the proportion of allochems and
516 matrix within samples, and differences in the source of fluids involved in the precipitation and
517 diagenetic stabilization of matrix components. Specifically, Present et al. (2015) suggest that
518 precipitation of micritic components from reduced pore fluids at or near the sediment water
519 interface could greatly influence the isotopic composition of CAS (see also Higgins et al., 2009
520 for a similar argument with respect to carbon isotopes).
521 Sulfur isotope compositions of CAS recorded in sections from Argentina, Newfoundland,
522 and South China are similar, ranging primarily between +10 and +30‰ (Table 1; Figs. 7, 8, 9,
523 10), and average compositions for different measured sections of the same unit are remarkably
524 similar (e.g., San Juan at La Silla $\delta^{34}S_{CAS}$ = 21.1 ±3.7‰; San Juan at La Chilca $\delta^{34}S_{CAS}$ = 20.5
525 ±3.8‰; San Juan at Talacasto $\delta^{34}S_{CAS}$ = 22.8 ±3.3‰). Despite this general similarity, there are
526 also conspicuous stratigraphic and regional differences in isotopic compositions (*see summary*
527 Fig. 10).
528 CAS from both the Argentine Precordillera and western Newfoundland, for instance,
529 record a rapid approximately 6-8‰ variation through much of the sampled section (Figs. 7, 8).
530 This short-term variation has been interpreted by Thompson and Kah (2012) to reflect deposition

531 near a marine chemocline, with isotopically heavy values representing deposition from ambient
532 seawater and isotopically light values representing the transient input of isotopically light sulfur
533 during sulfide oxidation at the chemocline (see section 4.1.1.). Such isotopic variation is
534 consistent with the hypothesis of Present et al. (2015) that fine-grained components may reflect
535 distinct sources of sulfate during deposition and early diagenetic stabilization. It is less likely that
536 such substantial isotopic variation could result from the systematic variation in the percentage of
537 allochems within the rock; using values from Present et al. (2015), variation in fossil (bryozoan-
538 echinoderm) concentration between 10-40% would only result in a 2‰ change in isotopic
539 composition of the bulk rock. Furthermore, in South China, despite similarity in bulk rock
540 composition, such rapid variation occurs only in the lower, shallower-water portions of the
541 succession, and is absent from deeper-water strata from the Yangtze Platform (Fig 9), suggesting
542 that changes in isotopic composition reflect compositional differences associated with water
543 depth.
544 Additionally, CAS from both the Argentine Precordillera and western Newfoundland
545 record an abrupt 10‰ drop in the average isotopic composition of CAS from near 25‰ (30‰ in
546 western Newfoundland) to approximately 15‰ (20‰ in western Newfoundland) in the lower
547 Darriwilian. This 10‰ change isotopic composition is not transient, and reflects a change in the
548 average isotopic composition of CAS that is sustained for the rest of the Darriwilian—an interval
549 of nearly 8 million years. Such a large change in the isotopic composition of CAS cannot readily
550 be explained except via a fundamental change in the isotopic composition of source waters. Such
551 an abrupt drop in isotopic composition, however, is not apparent in samples from the Yangtze
552 platform (Fig 10), although there is a change in average isotopic composition from
553 approximately 30‰ in the early Dapingian to approximately 25‰ in the lower Darriwilian. As a

554 result, in the Darriwilian, CAS from the Yangtze Platform shows clear enrichment in ^{34}S
555 compared to both Argentina and Newfoundland.

556 In addition to CAS, sulfur isotope compositions were also measured in sedimentary pyrite
557 form the Las Chacritas and Las Aguaditas formations in Argentina, and in the Table Point and
558 lower Table Cove formations of the Table Head Group, western Newfoundland (Table 1; Fig.
559 11). Pryite sulfur is heavy and variable in both the Table Head Group ($\delta^{34}S_{PY}$ = 2.0 ±8.8) and in
560 the Las Chacritas Formation ($\delta^{34}S_{PY}$ = 1.4 ±6.8). Sulfur isotope composition of pyrite within the
561 Las Aguaditas Formation becomes even more extreme, but less variable ($\delta^{34}S_{PY}$ = 14.5 ±4.2).
562 These values result in a profile in which relatively positive values of $\Delta\delta^{34}S$ (i.e., the difference in
563 isotopic composition between CAS and pyrite) near 25‰ occur from the late Floian through the
564 Dapingian. Then, in the early Darriwilian, coincident with abrupt drop in the isotopic
565 composition of CAS, $\Delta\delta^{34}S$ gradually falls to values near -5‰. These anomalously low values of
566 $\Delta\delta^{34}S$ remain through much of the late Darriwilian and then gradually rise into the Sandbian (Fig.
567 11).
568
569 4.0. Discussion
570 *4.1. Sulfur isotope behavior*
571 The Early to Middle Ordovician epochs represent a global greenhouse interval (Berner,
572 1994) when high sea level (Haq and Schutter, 2008), extensive epeiric seas (Algeo and
573 Seslavinsky, 1995), and elevated sea surface temperatures (Trotter et al., 2008; Finnegan et al.,
574 2011) may have favored sluggish ocean circulation (Saltzman, 2005). Development of regional
575 anoxia under such conditions is expected to result from a combination of decreased oxygen
576 solubility in marine waters, oxygen consumption during organic matter decomposition, and

reduced ventilation of deep-ocean environments (Sarmiento et al., 1988; Meyer and Kump, 2008). In turn, anoxic marine conditions would reduce potential for reoxidation of microbially produced hydrogen sulfide (Jørgensen et al., 1990) and favor development of regional euxinia. Several aspects of the marine sulfur isotope record in the Ordovician have been previously used to suggest the presence of a euxinic marine reservoir. Here, we use the combination of the following observations to infer the presence of at least locally euxinic conditions, including (Fig 10, 11): (1) broad covariation of carbon and sulfur (CAS) isotope compositions in the Floian and Dapingian, (2) rapid fluctuation in the isotopic composition of marine sulfate (*see also* Thompson and Kah, 2012), (3) difference in the rate of change in the isotopic compositions of marine sulfate (CAS) and marine sulfide minerals in the Dapingian to early Darriwilian, and (4) a reduction in isotope variability and the occurrence of "superheavy" pyrite (cf. Ries et al., 2009) in the late Darriwilian.

4.1.1. Marine sulfate

Broad covariation of carbon and sulfur (CAS) isotope compositions is apparent in the Floian and Dapingian of both Argentina and South China. In Argentina, a 1.5‰ rise and fall in carbon isotope compositions between the early Floian and mid-Dapingian negative excursions is mirrored by a nearly 10‰ rise and fall in the average isotopic composition of CAS (Fig. 7; cf. Thompson and Kah, 2012). Similar covariation is even more readily apparent in South China, where a similar 1.5‰ rise and fall in carbon isotopes are mirrored by a >15‰ rise and fall in the isotopic composition of CAS (Fig. 9). Such covariation has been identified in Late Cambrian successions worldwide (Gill et al., 2011), including from western Newfoundland (Hurtgen et al.,

599 2005), where Ordovician covariation is less obvious (Fig. 8), as well as in other Ordovician
600 successions (Marenco et al., 2013; Edwards and Saltzman, 2014).

601 Long-term, parallel responses in both carbon and sulfur isotope records suggests a common
602 driver. Specifically, covariation was likely driven by changes in organic carbon burial and
603 related changes in pyrite burial. Although not uniquely necessary, direct linkage of the carbon
604 and sulfur cycles is a hallmark of euxinic conditions (Berner, 1984), wherein increased delivery
605 of organic carbon fuels microbial sulfate reduction in anoxic waters, resulting in expansion of
606 euxinic conditions. Within euxinic waters, reduced sulfur is ultimately converted to pyrite and
607 buried alongside residual organic carbon. The scarcity of oxidants in euxinic waters would also
608 have increased the burial efficiency of pyrite (Hurtgen et al., 2005), which is particularly
609 necessary when the fractionation between coeval sulfate and sulfide reservoirs ($\Delta\delta^{34}S = \delta^{34}S_{CAS}$
610 $- \delta^{34}S_{PY}$) is reduced, resulting in reduced C/S burial rates and ultimately leading to the larger
611 change in the isotopic composition of sulfur relative to carbon that are observed in these sections.

612 More strikingly than the apparent sympathetic behavior in marine carbon and sulfur
613 isotopes, is an apparent short-term oscillation in the isotopic composition of CAS, particularly in
614 samples from Argentina and Newfoundland (Figs. 7, 8). In a detailed analysis, Thompson and
615 Kah (2012) showed that such short-term variation, which represent oscillations of 6-8‰ over
616 periods of approximately 1 Myr, do not reflect obvious changes in depositional environment,
617 rock composition, or degree of postdepostional diagenesis. Such oscillations therefore appear to
618 represent a fundamental behavior of the marine sulfur system. Yet, despite evidence for low
619 marine sulfate concentrations (<2-10 mM) in the lower Paleozoic from a combination of fluid
620 inclusions in marine halite (Lowenstein et al., 2001, 2003; Brennan et al., 2004; Petrychenko et
621 al., 2005) and ^{34}S-enriched isotopic compositions of marine pyrite (Strauss, 1999; Gill et al.,

622 2007, 2011; Hurtgen et al., 2009), rates of isotopic change recorded in these oscillations are
623 inconsistent with traditional interpretations of the sulfur cycle. Rather high-frequency isotopic
624 variation suggests a combination of low sulfate concentration and non-conservative behavior of
625 marine sulfate (Thompson and Kah, 2012).

626 Steady-state and time-dependent models (Thompson and Kah, 2012) indicate that under
627 concentrations of marine sulfate as low as <2 mM, observed fluctuations would require either
628 systematic variation of >25‰ in the fractionation between oxidized and reduced sulfur reservoirs,
629 a 40% fluctuation in pyrite burial, periodic changes in the input flux of weathering by a factor of
630 2, or a >15‰ change in the composition of the weathering flux. Analysis of coeval sulfate and
631 sulfide phases (Fig. 11), however, do not support required variation in fractionation, and there is
632 no evidence to support dramatic, yet equivalent, changes in weathering flux in the geographically
633 disparate sections from Argentina and western Newfoundland. The presence of euxinic deep
634 waters, however, could provide a suitable reservoir of highly reactive, isotopically light sulfur,
635 which, if modeled as a potential input, could result in substantial changes in the isotopic
636 composition of marine sulfate. A scenario in which the percentage of HS^- that is oxidized is
637 permitted to fluctuate may also affect the efficiency of pyrite burial rates (Turchyn and Schrag,
638 2004; Hurtgen et al., 2005).

639 Interestingly, the isotopic profile of marine sulfate for the Yangtze platform, South China,
640 does not record clear evidence for periodic oscillation in the isotopic composition of marine
641 sulfate (Fig. 9). Potential oscillations of similar magnitude to that in the Argentina and western
642 Newfoundland sections occur in the Hunghuayuan and the lowermost Dawan formation, which
643 represent the shallower-water facies prior to a substantial marine transgression, but are
644 conspicuously absent for the remainder of the Dawan Formation. Such observation is consistent

with the presence of anoxic to sulfidic deep-waters if the majority of the Dawan Formation was deposited below a marine chemocline. Within an anoxic water column, microbial sulfide reduction occurs progressively, which results in the depletion of the standing sulfate reservoir and a progressive increase in hydrogen sulfide. In this scenario, the isotopic composition of sulfate in oxic surface waters would reflect the net removal of isotopically light sulfur during MSR. Beneath the chemocline, however, the isotopic composition of residual sulfate will depend on the position within the water column and the corresponding depletion of the residual sulfate reservoir (Saelen et al., 1993; Gomes and Hurtgen, 2013). If a portion of the standing hydrogen sulfide reservoir is allowed to oxidize, the overlying oxic water column will receive a rapid delivery of isotopically light sulfate and will, in turn, record isotopic change within CAS. Oxidation of a portion of the hydrogen sulfide reservoir, however, will not play a role in the isotopic composition of the residual sulfate reservoir within the anoxic zone, and CAS incorporated into carbonate minerals beneath the chemocline will instead record the composition of residual sulfate at the point of deposition (cf. Gomes and Hurtgen, 2013).

4.1.2. Marine sulfide

Sulfur isotope compositions of coeval sulfate and sulfide were measured from the Las Chacritas and Las Aguaditas formations in Argentina, and in the Table Point and lower Table Cove formations of western Newfoundland (Fig. 11). In the marine system, the difference in sulfur isotope composition between marine sulfate (as derived from CAS) and sulfide (as derived from sedimentary pyrite) reservoirs ($\Delta\delta^{34}S = \delta^{34}S_{CAS} - \delta^{34}S_{PY}$), primarily reflects isotopic fractionation deriving from bacterial sulfate reduction and its associated intermediate redox metabolisms, such as sulfur disproportionation which typically result in depletion of sulfide

668 relative to coeval sulfate (Canfield and Teske, 1996; Canfield, 2001). The magnitude of
669 fractionation, however, also reflects the size of the available sulfate reservoir (Lyons et al., 2009),
670 whether precipitation of solid-phase sulfide minerals occurs diagenetically within the substrate,
671 or syngenetically within the water column, and even the position of pyrite formation within a
672 euxinic water column (Gomes and Hurtgen, 2013).

673 The presence of persistent euxinia in the Ordovician is supported by both the isotopic
674 composition and the long-term isotopic behavior of marine sulfide minerals. The isotopic
675 composition of sedimentary pyrite in these sections is quite variable, ranging from approximately
676 -20‰ to +20‰ through the section. At least some of this variability is likely to reflect variability
677 in the parent sulfate reservoir, because the difference in fractionation between sulfate and sulfide
678 ($\Delta\delta^{34}S$) shows substantially less variability. For example, during the middle Dapingian, $\Delta\delta^{34}S$
679 remains relatively constant near 25‰. Although this value is substantially less than the >40‰
680 common in modern marine systems, it is consistent with fractionations observed during times of
681 globally low marine sulfate, including the lower Paleozoic (Kah et al., 2001; Gill et al., 2007,
682 2011; Hurtgen et al., 2009). Values of $\Delta\delta^{34}S$ also remain relatively steady during the Dapingian,
683 which suggests syngenetic production of sedimentary sulfide minerals within a euxinic water
684 column; when sulfide mineral production is restricted to diagenetic environments within the
685 substrate, limitations of sulfate availability result in heavier and more isotopically variable
686 compositions of sedimentary pyrite (Lyons et al., 2009).

687 An intriguing shift in the isotopic composition of sedimentary sulfide (and its concomitant
688 effect on $\Delta\delta^{34}S$) observed during the middle Dapingian of these sections (Fig. 11) is also
689 consistent with development of euxinic conditions at these localities. In the middle Dapingian,
690 the sulfur isotope composition of sedimentary pyrite increases sharply to nearly 20‰. This

691 isotopic shift is also observed as a 15‰ decrease in $\Delta\delta^{34}S$. In this example, however, there is
692 little evidence of sympathetic behavior in the isotopic composition of marine carbon, which
693 experiences a coeval negative shift, or in the isotopic composition of marine sulfate, which
694 records little difference other than in potential increase in the magnitude of short-term isotopic
695 variability (Fig. 11). Such behavior is distinct from the longer-term sympathetic behavior
696 observed in other lower Paleozoic successions (Gill et al., 2011). Antithetical behavior between
697 the isotopic composition of marine carbon and marine sulfide minerals can best be explained by
698 a transient decrease in marine productivity and organic carbon delivery that is not balanced by
699 changes in pyrite production. In this scenario, decoupling of organic carbon delivery from MSR
700 requires the presence of a euxinic reservoir that contains sufficient organic carbon to drive
701 continued MSR. The marked decrease in $\Delta\delta^{34}S$ further indicated that, during this interval,
702 consumption of marine sulfate within the anoxic zone exceeded the rate of supply, resulting in
703 near complete depletion of sulfate within the anoxic zone (i.e. greater degree of euxinia) (cf.
704 Gomes and Hurtgen, 2013). Absence of a sympathetic increase in the isotopic composition of
705 marine sulfate, however, suggests that this transient activity was not necessarily reflected in
706 increased pyrite burial. Changes in the degree of euxinia (i.e., the extent to which residual sulfate
707 in the anoxic zone is depleted), however, could potentially affect the flux of isotopically light
708 sulfate introduced during short-term oxidation events, which would result in a larger magnitude
709 of isotopic change of sulfate within the oxic surface reservoir.
710 In addition to the short-term change in sulfide isotopic composition in the middle
711 Dapingian, strata from Argentina and Newfoundland also record a long-term, 30‰ shift in the
712 isotopic composition of marine sulfide beginning in the early Darriwilian (Fig. 11). This shift, in
713 which average isotopic compositions of marine sulfide (as recorded in sedimentary pyrite) start

714 near –10‰ and climb steadily to average values near 20‰, is marked by a concomitant decrease
715 in $\Delta\delta^{34}S$ from 25‰ to –5‰, which marks deposition of "superheavy" pyrite (*see below*). This
716 long-term shift in the isotopic composition of marine sulfide is coincident with a sharp, 30‰
717 decrease in the isotopic composition of sulfate (Fig. 11). The difference in the direction of these
718 30‰ shifts, however, requires that marine sulfate and sulfide reservoirs be decoupled with
719 respect to their isotopic compositions, wherein ^{34}S-depleted values in marine sulfate are not
720 translated directly via MSR and pyrite formation to marine pyrite. Similarly, the difference in the
721 rate of change in isotope composition between marine sulfate and marine sulfide minerals
722 requires that the marine sulfide reservoir does not experience reservoir effects to the same extent
723 as at the marine sulfate reservoir. This suggests the presence of a marine sulfide reservoir greater
724 in magnitude than that of marine sulfate (cf. Rothman et al., 2003), which does not seem likely in
725 the absence of substantial, water-column euxinia..
726
727 *4.1.3. Superheavy pyrite*
728 As noted above, a 30‰ long-term shift in the isotopic composition of marine sulfide
729 minerals results in the formation of "superheavy" pyrite. By contrast to most normal marine
730 systems, in which the isotopic composition of pyrite is depleted in ^{34}S relative to coeval sulfate,
731 superheavy pyrite is defined as a negative fractionation between sulfate and sulfide reservoirs
732 ($\Delta\delta^{34}S = \delta^{34}S_{CAS} - \delta^{34}S_{PY}$), wherein the reduced sulfur phase is isotopically enriched relative to
733 coeval sulfate. Superheavy pyrite is observed within the Las Aguaditas Formation throughout the
734 latest Darriwilian (Fig. 11), where the sulfur isotope composition of sedimentary pyrite is
735 consistently enriched relative to that of CAS (averaging $\Delta\delta^{34}S$= -5‰). Superheavy pyrite has
736 been reported numerous times in the Proterozoic, particularly in the late Neoproterozoic (Xu et

al., 1990; Li et al., 1999; Gorjan et al., 2000; Bottomley et al., 1992; Hayes et al., 1992; Strauss et al., 1992; Tie-bing et al., 2006; Shen et al., 2008; McFadden et al., 2008; Ries et al., 2009) and in the Paleoproterozoic aftermath of the Great Oxidation Event (Thode et al., 1962; Hayes et al., 1992; Shen et al., 2002), and, most recently, from the late Cambrian (Gill et al., 2011) and the late Devonian (Chen et al., 2013; Sim et al., 2015).

Superheavy pyrite within glacially-affected strata in the Neoproterozoic has been attributed to Rayleigh distillation within a sulfate-poor water body decoupled from overlying sulfate-rich waters within physically stratified ocean waters (Tie-bing et al., 2006; Shen et al., 2008). Elsewhere, where abundant storm-generated beds restrict the potential for persistent physical stratification, the occurrence of superheavy pyrite has been attributed to intense aerobic reoxidation of marine sulfide (Ries et al., 2009). In an alternative model, superheavy pyrite associated with the late Devonian Alamo impact breccia has been attributed to the stripping and release of hydrogen sulfide from sediment pore waters during catastrophic disturbance of the sea bed (Sim et al., 2015). Although Sim et al. (2015) ascribe superheavy pyrite to reservoir effects associated with continued MSR within the sediment profile, a scenario of catastrophic release of porewater hydrogen sulfide could also result in enhanced aerobic rexoidation within the water column. Aerobic oxidation of hydrogen sulfide (HS^-)—either within pore waters or within the water column—could produce oxidized sulfur species, such as sulfate ($SO_4^=$), that are depleted relative to the parent sulfide by up to 5‰ (Fry et al., 1988; up to 18‰ for bacterial oxidation, Kaplan and Rittenberg, 1964). Effects of this fractionation would be minimal in a marine environment where mass-dependent fractionation during MSR reached modern values of >46‰ (Canfield and Thamdrup, 1994; Habicht et al., 1998), but could have been substantial when fractionation imparted during MSR was restricted by low seawater sulfate concentrations, such

760 as in the Ordovician (Thompson and Kah, 2012; Marenco et al., 2013). Notably, all occurrences
761 of superheavy pyrite in the Proterozoic occur at times where marine geochemical indicators
762 independently indicate the presence of a persistent, euxinic water body (Poulton et al., 2004;
763 Brocks et al., 2005; Fike et al., 2006; Scott et al., 2008; Li et al., 2010).
764
765 *4.2 Dual-reservoir model*
766 Data provided here suggest that regional euxinic conditions likely persisted through at least
767 the Middle Ordovician. The presence of persistent euxinia requires a mechanism of modeling
768 marine sulfur that moves away from traditional single reservoir steady state and time-dependent
769 analyses (cf. Thompson and Kah, 2012). A dual-reservoir model (cf. Rothman et al., 2003),
770 however, considers the existence of two distinct reservoirs for sulfur in the marine system: an
771 oxic reservoir dominated by sulfate, and an anoxic reservoir within which sulfate is actively
772 reduced to hydrogen sulfide and all transient reduced sulfur species (Fig. 12). In this case, the
773 size and isotopic composition of the oxic reservoir is controlled not only by the input flux from
774 crustal weathering and the output flux from sulfate deposition (as gypsum or CAS), which act
775 over long time-scales, but also by a suite of transitory fluxes that include depletion of the oxic
776 reservoir via MSR and by potential input driven by oxidation of the anoxic reservoir. The
777 isotopic composition of these fluxes will, in turn, reflect a combination of the redox pathway,
778 and the composition and size of the respective reservoirs. Additionally, oxidation of the
779 hydrogen sulfide reservoir may be driven by either chemical or biological sulfide oxidation. In
780 terms of the model application, although these chemical and biological sulfide oxidation
781 pathways are associated with substantially different fractionations (Kaplan and Rittenberg, 1964;

782 Fry et al., 1988), difficulty in distinguishing oxidation pathways can, for simplicity, be reflected
783 in condensation of these terms to a single oxidation flux.

784 A critical difference between single and dual reservoir models is that, in a single reservoir
785 model, pyrite burial—with its large associated fractionations—is often taken to be the primary
786 driver of changes in the isotopic composition of marine sulfate. By contrast, a dual-reservoir
787 model requires that the isotopic composition of the marine sulfate reservoir be influenced
788 directly by pyrite burial only when the fluxes between the two reservoirs (i.e., MSR and sulfide
789 oxidation) are in equilibrium, or under conditions of enhanced marine oxygenation, when rapid
790 reoxidation of microbially reduced hydrogen sulfide and its sulfur intermediates (cf. Jørgensen et
791 al., 1990) effectively depletes the sulfide reservoir that is not immediately incorporated into
792 sedimentary pyrite. When MSR outpaces sulfide oxidation and sedimentary pyrite formation,
793 pyrite burial and MSR become decoupled. This decoupling represents a dynamically maintained
794 disequilibrium between the oxic and anoxic reservoirs, wherein the rate processes acting as
795 fluxes between the two reservoirs is critical to understanding the relative behavior of the
796 reservoirs (Rothman et al., 2003).

797 Evaluation of Figure 12 permits construction of equations that govern both the isotopic
798 composition (δ_{SO4}, δ_{HS}) and the size (M_{SO4}, M_{HS}) of the distinct, chemically active reservoirs:
799 sulfate [$SO_4^{=}$] and reduced sulfur [HS^-], the latter of which includes all transient reduced sulfur
800 species. Fluxes and their isotopic compositions include input from crustal weathering (F_W, δ_W);
801 output via deposition of sedimentary sulfur as gypsum (F_{GYP}, δ_{GYP}), carbonate-associated sulfate
802 (F_{CAS}, δ_{CAS}), or pyrite (F_{PY}, δ_{PY}); as well as microbial sulfur reduction with or without expression
803 of sulfur disproportionation (F_{MSR}, δ_{MSR}), abiotic sulfide oxidation (F_{OX}, δ_{OX1}), and biological
804 sulfide oxidation (F_{OX}, δ_{OX2}), where the isotopic compositions of sulfur reduction and oxidation

are expressed as a difference in composition between the reservoir and the composition imparted by fractionation that occurs during the respective reduction or oxidation process (ε_{MSR}, ε_{OX}), wherein $\delta_{MSR} = \delta_{SO4} - \varepsilon_{MSR}$, $\delta_{OX1} = \delta_{HS} - \varepsilon_{OX(abiotic)}$, and $\delta_{OX2} = \delta_{HS} - \varepsilon_{OX(biotic)}$. For simplification, output as sedimentary gypsum or CAS is combined into a single flux (F_{CaSO4}, δ_{CaSO4}), and redox reactions are also simplified to single reduction and oxidation parameters (F_{MSR}, ΔS_{MSR}) and (F_{OX}, Δ_{OX}).

Change in the isotopic composition of each reservoir reflects both the mass of the reservoir and the input and output fluxes from that reservoir. For the marine sulfate reservoir:

$$d\delta_{SO4}/dt = 1/M_{SO4} [F_W(\delta_W - \delta_{SO4}) + F_{OX}(\delta_{OX} - \delta_{SO4}) - F_{MSR}(\delta_{MSR} - \delta_{SO4}) - F_{CaSO4}(\delta_{CaSO4} - \delta_{SO4})]. \quad (2)$$

Note that because the output of marine sulfate to the solid phases of gypsum and CAS typically show little fractionation from their parent marine sulfate reservoir (Raab and Spiro, 1991), the final term of this equation will go to zero unless there is evidence of substantial gypsum deposition. Additionally, the equation can be rewritten in terms of fractionation factors (ε_{MSR} and ε_{OX}), such that:

$$d\delta_{SO4}/dt = 1/M_{SO4} [F_W(\delta_W - \delta_{SO4}) + F_{OX}(\delta_{HS} - \varepsilon_{OX} - \delta_{SO4}) + F_{MSR}(\varepsilon_{MSR})]. \quad (3)$$

Similarly, for the marine reduced sulfur reservoir:

$$d\delta_{HS}/dt = 1/M_{HS} [F_{MSR}(\delta_{MSR} - \delta_{HS}) - F_{OX}(\delta_{OX} - \delta_{HS}) - F_{PY}(\delta_{PY} - \delta_{HS})]. \quad (4)$$

As with before, because output of marine pyrite shows little fractionation from their parent marine sulfide reservoir, the final term of this equation will go to zero. When rewritten in terms of fractionation factors (ε_{MSR} and ε_{OX}), the equation becomes:

$$d\delta_{HS}/dt = 1/M_{HS}\,[F_{MSR}(\delta_{SO4} - \varepsilon_{MSR} - \delta_{HS}) + F_{OX}(\varepsilon_{OX})]. \quad (5)$$

In the case where fluxes are either constrained or modeled, evolution of the mass of these reservoirs can similarly be examined, wherein:

$$dM_{SO4}/dt = F_W + F_{OX} - F_{MSR} - F_{CaSO4} \quad (6)$$

and

$$dM_{HS}/dt = F_{MSR} - F_{OX} - F_{PY} \quad (7)$$

4.2.1. Dual-reservoir characteristics of the Darriwilian

Sulfur isotope data from Newfoundland and Argentina record an abrupt and dramatic shift in the average isotopic composition of marine sulfate from approximately 30‰ to 15‰ in the early Darriwilian (c. 467 Ma) of Newfoundland, and from approximately 25‰ to 15‰ in Argentina (Fig. 10). This 10 to 15‰ shift marks a profound perturbation in the isotopic composition of marine sulfate that is not compensated by an equivalent shift in the isotopic composition of sedimentary pyrite. Furthermore, this shift is estimated to occur over <500 Ky,

851 which is approximately half the duration of the much smaller isotopic fluctuations that
852 characterize these successions (Thompson and Kah, 2012). In the aftermath of this dramatic
853 perturbation, the isotopic composition of both marine C and pyrite S increase over approximately
854 4 My (see Fig. 11). In the case of marine pyrite, a 30‰ shift in the isotopic composition of pyrite
855 ultimately culminates in an interval of superheavy pyrite marked by unusual inverse fractionation
856 between sulfate and sulfide reservoirs that persisted for >3 Myr, into the Late Ordovician (Fig.
857 11).

858 Both the dramatically different response times recorded in marine sulfate and sulfide, and
859 the occurrence of superheavy pyrite are evidence for dynamic disequilibrium between oxidized
860 and reduced water masses. When considering a dual reservoir system, disequilibrium in both the
861 size of the reservoirs and the fluxes between the two reservoirs results in the relative behavior of
862 the reservoirs (Rothman et al., 2003). Fluxes larger than that inferred by the residence time of the
863 smaller reservoir carry the potential to dramatically affect isotopic composition of the smaller
864 reservoir. Similarly, fluxes smaller than that inferred by the residence time of the larger reservoir,
865 will have a protracted, rather than immediate effect on the isotopic composition of the larger
866 reservoir. We suggest that the observed, early Darriwilian isotope events recorded in
867 Newfoundland and Argentina resulted from a rapid flux of oxidized hydrogen sulfide to surface
868 waters. The effects of this flux are observed as a dramatic, short-term change in the isotopic
869 composition of marine sulfate (Fig. 11). By contrast, a similar size shift in the composition of the
870 marine sulfide reservoir (as measured by the composition of marine pyrite) occurs over a much
871 longer period, suggesting that the standing marine sulfide reservoir was substantially larger than
872 the local marine sulfate reservoir.

873 The presence of superheavy pyrite is also a direct consequence of oxidation of the marine
874 hydrogen sulfide reservoir. Oxidation of hydrogen sulfide produces oxidized sulfur species that
875 are depleted relative to the parent sulfide by 5‰ to 18‰ (Fry et al., 1988; Kaplan and Rittenberg,
876 1964). Continued MSR within the remaining anoxic reservoir will drive hydrogen sulfide to
877 isotopically heavier values, and potentially, even in the absence of Rayleigh fractionation effects,
878 to isotopic compositions heavier than marine sulfate in the associated oxic reservoir.
879 Furthermore, if we reasonably assume that rapid fluctuation in the marine sulfate reservoir
880 reflects small, yet high frequency oxidation events (Thompson and Kah, 2012), the dramatic
881 reduction in the magnitude of these fluctuations during the interval of superheavy pyrite
882 production suggests potential for near complete removal of HS^- as pyrite, or a potential loss of
883 the euxinic water body. Return of higher-magnitude fluctuations in the early Late Ordovician
884 would then mark reestablishment of euxinic conditions.
885
886 4.2.2. Estimating reservoir size
887 Although a dual-reservoir model provides an important scenario within which to interpret
888 observed patterns of isotopic change in the early Darriwilian, it is not straightforward to use this
889 model in terms of calculating the sizes of the respective oxidized and reduced sulfate reservoirs.
890 As with calculations based on a single reservoir model (cf. Kah et al., 2004), the marine sulfate
891 reservoir is here assumed to reflect globally connected, well-mixed marine surface waters.
892 Locally restricted environments, such as nearshore environments or within epeiric seaways, may
893 vary from well-mixed surface waters in terms of both sulfate concentration and isotopic
894 composition. Similarly, when applying a dual reservoir model to exploration of the size of a
895 marine sulfide reservoir, there is an inherent assumption of a globally connected euxinic water

896 body. We emphasize that the data provided here do not clearly define conditions of global
897 euxinia, but rather express that conditions suitable for development of euxinia occurred along
898 geographically disparate continental margins during the Ordovician, consistent with earlier
899 arguments on the limits of marine euxinia (Dahl et al., 2010; Gill et al., 2011; Reinhard et al.,
900 2013). Therefore, calculations of sulfide reservoir size that, by default, consider global euxinia
901 must be considered not in terms of discrete calculated masses, but rather in terms of molality.
902 Assuming that the marine sulfate reservoir corresponds to well mixed surface waters, we
903 can use a steady-state model to approximate the mass of the marine sulfate reservoir. Maximum
904 rates of isotopic change within the reservoir are reached when input of sulfate to the system
905 approaches zero and the standing marine sulfate reservoir is removed in its reduced form. In the
906 dual reservoir model provided here, we assign the weathering input of sulfate to the marine
907 system as zero (Fw = 0), assign influx from oxidation of hydrogen sulfide as zero ($F_{OX} = 0$), and
908 assign the primary driver of isotopic change to be the export of sulfate via microbial sulfur
909 reduction, wherein $F^* = F_W = 1.5x10^{18}$ mol/My (Kurtz et al., 2003). Equation 3 thus reduces to be
910 equivalent to a single reservoir model:
911
912 $$d\delta_{SO4}/dt = 1/M_{SO4}\,[F^*(\varepsilon_{MSR})]. \quad (8)$$
913
914 If we then assume that the observed rate of isotopic change (10-15‰ over a maximum of
915 500 Ky) records the maximum possible rate of change, and use the observed fractionation
916 between sulfate and sulfide as the fractionation factor, the isotopic shift recorded in early
917 Darriwilian CAS suggests a maximum sulfate reservoir size of approximately 1.5 to 2.25 $x10^{18}$

mol (or approximately 1-2 mM), and potentially less if isotopic compositions record only a fraction of maximum isotopic change (cf. Luo et al., 2015).

We can also estimate the relative amount of hydrogen sulfide that must have been oxidized to result in the observed change in the isotopic composition of marine sulfate. In this case, we will turn to the more simplistic single-reservoir model. A critical difference between single- and dual-reservoir models is that, in a single-reservoir model, the pyrite burial flux (F_{PY}) is presumed to reflect all byproducts of MSR that are not immediately reoxidized to sulfate and intermediate sulfide species. In a dual-reservoir model, fluxes acting between the two reservoirs (i.e. MSR and sulfide oxidation) are decoupled from pyrite burial in such a way that the MSR flux (F_{MSR}) reflects all byproducts of MSR that are not immediately reoxidized to sulfate (that is, the flux of HS^- available for sulfide oxidation, F_{OX}), and F_{PY} reflects only sulfide species that are transformed into the solid phase as pyrite. In this case, an estimate of the oxidized flux (F_{OX}) can be determined by modeling a single-reservoir steady-state pyrite flux before and after the observed change in the isotopic composition of the sulfate reservoir. In order to compensate for the second reactive reservoir, pyrite flux *before* the isotopic change in marine sulfate is set to equal the combined fluxes of pyrite and MSR ($F_1 = F_{PY} + F_{MSR}$). Additionally, pyrite flux *after* the isotopic change in marine sulfate is set to equal the combined fluxes of pyrite and MSR less the flux of oxidized sulfide ($F_2 = F_{PY} + F_{MSR} - F_{OX}$). Our results indicate that approximately 1.5×10^{18} mol (or 1 mM) of hydrogen sulfide—an amount nearly equal to the initial size of the sulfate reservoir—was oxidized during this event. Such calculation, even when regional euxinia is considered, is consistent with the existence of a large standing reduced sulfur reservoir.

Remembering the caveat that dual-reservoir modeling assumes a single global euxinic reservoir, the mass of the reactive sulfide reservoir (and its molality) can be similarly estimated.

941 Maximum rates of isotopic change are reached when input of hydrogen sulfide to a euxinic water
942 body via MSR approaches zero and the standing reservoir is removed via sulfide oxidation. In
943 the dual reservoir model provided here, we therefore assign MSR to be zero ($F_{MSR} = 0$), and
944 assign the primary driver of isotopic change to be the export of sulfate via a combination of
945 abiotic and microbial sulfur oxidation (F^*). Equation 5 thus becomes:
946
947 $$d\delta_{HS}/dt = 1/M_{HS}\,[F^*(\varepsilon_{OX})]. \quad (9)$$
948
949 Unfortunately, in this case, both the oxidation flux (F^*) and the potential fractionation during
950 sulfur oxidation are unknown. In the modern, up to 95% of sulfide is reoxidized to sulfate and
951 intermediate sulfur species prior to deposition as marine pyrite (Jørgensen et al., 1990),
952 indicating that marine sulfate reduction greatly outpaces pyrite deposition. Interestingly,
953 hypothesized rates of marine pyrite burial in the Phanerozoic ($6.7x10^{17}$ mol/My; Gill et al., 2011)
954 reflect approximately 6% of modern global sulfate reduction rates, calculated to be
955 approximately $11.3x10^{18}$ mol/My (Bowles et al., 2014). This observation suggests that pyrite
956 burial through geologic time is controlled primarily by the availability of reduced iron species,
957 and potentially lower rates of sulfur oxidation under low oxygen conditions of the geologic past
958 would simply be reflected in expansion of euxinic conditions. For calculation of the maximum
959 possible size of a global reduced sulfur reservoir, we therefore assume that all microbial sulfate
960 reduction is retained as marine euxinia, and we assign sulfur oxidation flux (F^*) to approximate
961 global sulfur reduction rates ($11x10^{18}$ mol/My). We expect that the standing size of the reduced
962 sulfur reservoir would have been lower than these maximum calculated values, depending on the
963 degree to which MSR is retained as water column euxinia.

964 Using the observed rate of isotopic change of marine pyrite (30‰ over an interval longer
965 than 3 My; Fig. 11) as the maximum rate of change, we can then calculate the size of the reduced
966 sulfur reservoir for either abiotic sulfur oxidation (ε_{OX} = 5‰; Fry et al., 1988), bacterial
967 oxidation (ε_{OX} = 15‰; Kaplan and Rittenberg, 1964), or a mixture of the two (ε_{OX} = 10‰).
968 Using equation 8, the isotopic shift recorded in early Darriwilian pyrite suggests a maximum
969 possible reduced sulfur reservoir of between 7.3×10^{18} mol (or 5.6 mM, for ε_{OX} = 5‰) and
970 2.2×10^{19} mol (or 17 mM, for ε_{OX} = 15‰). Locally, concentrations of hydrogen sulfide of 5.6 to
971 17 mM represent a standing sulfide reservoir approximately 3-8X the concentration of marine
972 sulfate (<2 mM).
973 As predicted by the patterns of behavior recorded in marine sulfate and sulfide,
974 calculations of reduced sulfur reservoir size are substantially larger than that calculated for
975 marine sulfate. A relatively large reduced sulfur reservoir, however, is consistent with the
976 dramatic difference in the response time of marine sulfate and marine sulfide at the time of this
977 early Darriwilian perturbation (cf. Rothman et al., 2003). Furthermore, in the case of dominantly
978 abiotic sulfide oxidation, these calculations would suggest that approximately 6-18% of the
979 standing sulfide reservoir (1 mM oxidized of a reservoir consisting of 5.6 mM to 17 mM
980 hydrogen sulfide) was oxidized during this event. If only a portion of MSR is retained as euxinia,
981 this event may represent an even greater extent of oxidation.
982
983 *4.3. Implications of oceanic ventilation*
984 Isotopic records of marine sulfate that are presented here suggest persistence of euxinic
985 conditions along continental margins through at least the Middle Ordovician. Dramatic changes
986 in the behavior of both marine sulfate and sulfide in the early Darriwilian point to an oxidation

event wherein a substantial portion of euxinic waters were oxidized over a short interval of time. Ventilation of these euxinic waters had an immediate effect on the isotopic composition of sulfate within oxic surface waters. Ventilation also occurred coincident with initial carbon isotope trends associated with the globally recognized MDICE excursion (Ainsaar et al., 2004; 2010; Kaljo et al., 2007; Bergstrom et al., 2008; Schmitz et al., 2010; Thompson et al., 2012; Albanesi et al., 2013; Sial et al., 2013). Observed records of C and S can plausibly be linked through enhanced nutrient delivery to the oceans (cf. Saltzman et al., 2005; Thompson and Kah, 2012), wherein oceanic ventilation reduced N-limitation stimulated organic productivity.

Data presented here also may lend new insight into the complex linkages between Ordovician ocean chemistry and climate by providing a temporal framework for understanding biospheric responses to deep ocean ventilation. Elevated sea surface temperatures (SSTs) during greenhouse climates of the early Middle Ordovician resulted in sluggish oceanic circulation, enhanced ocean anoxia and maintenance of a substantial HS^- reservoir. We suggest that disequilibrium conditions observed within the marine sulfur isotope record resulted from oxidation of a deep-water HS^- reservoir. The onset of this ventilation event occurs coincident with marine equatorial SSTs reaching their lowest point in more than 25 My (Trotter et al., 2008). From this perspective, it seems plausible that lower equatorial SSTs reflect global cooling in the Darriwilian, intensified thermohaline circulation, and potential delivery of cool, oxygenated waters to deeper portions of the water column..

Ventilation of the water column, however, is shown here to have begun in the early Darriwilian, nearly 10 My earlier than the traditional onset of glacial climates. Climate deterioration is a hallmark of the terminal Ordovician (Brenchley et al., 1994; Delabroye and Vecoli, 2010; Finnegan et al. 2011), which is marked by widespread glaciation on Gondwana

and a catastrophic loss of marine diversity (Sheehan, 2001; Harper et al., 2013). The transition to icehouse conditions, however, may have occurred as early as the Katian, as marked by oceanic ventilation, enhanced productivity, and atmospheric CO_2 drawdown (Pope and Steffen, 2003; Tobin et al., 2005; Saltzman and Young, 2005; Lefebvre et al., 2010; Young et al., 2010; see alternate view in Quinton and MacLeod, 2014). Together, results from this study and other recent studies (Jones and Fike, 2013) suggest a dynamic and rapidly evolving Ordovician system sensitive to environmental perturbations, wherein long-term cooling initiated in the Darriwilian ultimately progressed into full-scale glaciation and mass extinction some 25 Myr later.

5. Conclusions

1. The marine sulfur isotope record is critical to deciphering both the long-term oxygenation of the Earth's surface and the evolution of the Earth's oceans. Oxygenation of the Earth's oceans, in particular, has dramatic effects on the distribution of bioessential trace elements and, thus, on the distribution and evolution of life in the oceans.
2. Much of our current understanding of marine oxygenation relies on our interpretation of marine sulfur based on a single reservoir model. In this model, isotopic composition of marine sulfate (as measured via CAS) is controlled primarily by the production and burial of sedimentary pyrite. Modifications to this single reservoir model, including investigation of non-steady state properties, has increased the utility of the model, although the model remains of limited use at times of exceedingly small reservoir size, and during times of persistent marine euxinia.
3. Persistent marine euxinia marks a fundamental decoupling between oxic and anoxic marine reservoirs. At such times, short-term fluxes that act between the two reservoirs

(i.e., MSR and sulfide oxidation processes) often dominate over the longer term fluxes (i.e. weathering and pyrite burial) that control the single reservoir model.

4. Ordovician strata from Argentina, western Newfoundland, and South China illustrate a range of effects driven by the presence of local euxinia. Over multimillion-year time scales, covariance between the isotopic composition of marine carbon and sulfur provide evidence of nutrient feedbacks. The position of marine carbonate deposition within the water column, however, can result in substantial differences in sulfur isotope behavior over million-year time scales: whereas carbonate precipitated above a regional chemocline can preserve rapid fluctuation in S-isotope composition, reflecting short-term disequilibrium between oxic and anoxic reservoirs, carbonate precipitated below a regional chemocline will record the extent to which MSR has depleted residual sulfate in the anoxic zone.
5. A dramatic reorganization of the sulfur isotope record in the early Darriwilian reflects dynamic disequilibrium between oxic and anoxic marine reservoirs driven by ventilation of euxinic water. Ventilation and oxidation of euxinic reservoirs result in a rapid change in the isotopic composition of marine sulfate in surface oceans, and ultimately drove the near complete depletion of the hydrogen sulfide within the anoxic reservoir. Depletion of euxinia is marked by superheavy pyrite formation and a loss of the characteristic short-term isotopic fluctuation of marine sulfate. Ventilation occurs coincident with the lowest SSTs in more than 25 My and may represent the onset of climatic change that ultimately led to late Ordovician glaciation.

Acknowledgements

Funding was provided by the National Geographic Society (NGS 7866-05 to Kah), the National Science Foundation (NSFEAR 0745768 to Kah), and the American Chemical Society (ACS-PRF 48166 to Kah), along with student grants from Sigma Xi, the Geological Society of America, and SEPM (to Thompson). We give special thanks to R. Astini and F. Gomez, and G. Gilleaudeau for help in conducting field work; and L. Pratt, A. Szynkiewicz, and M. Peretich for help with isotopic and elemental analyses. M. Hurtgen, B. Gill, and P. Marenco provided careful and thoughtful reviews that aided in the clarity of this manuscript.

References

Ainsaar, L., Meidla, T., Tinn, O., 2004. Middle and Upper Ordovician stable isotope stratigraphy across the facies belts in the East Baltic. In: Hints, O., Ainsaar, L. (Eds.), WOGOGOB-2004 Conference Materials. Tartu University Press, Tartu, pp. 11–12.

Ainsaar, L., Kaljo, D., Martma, T., Meidla, T., Männik, P., Nõlvak, J., Tinn, O., 2010. Middle and Upper Ordovician carbon isotope chemostratigraphy in Baltoscandia: a correlation standard and clues to environmental history. Palaeogeography, Palaeoclimatology, Palaeoecology 294, 189–201.

Albanesi, G.L., Bergström, S.M., Schmitz, B., Serra, F., Feltes, N.A., Voldman, G.G., Ortega, G., 2013. Darriwilian (Middle Ordovician) δ^{13}Ccarb chemostratigraphy in the Precordillera of Argentina: Documentation of the middle Darriwilian Isotope Carbon Excursion (MDICE) and its use for intercontinental correlation. Palaeogeography, Palaeoclimatology, Palaeoecology 389, 48-63.

1077 Algeo, T.J., Seslavinsky, K.B., 1995. The Paleozoic world; continental flooding, hypsometry,
1078 and sea level. American Journal of Science 295, 887-822.

1079 Algeo, T.J., Luo, G.M., Song, H.Y., Lyons, T.W., Canfield, D.E., 2014. Reconstructyion of
1080 secular variation in seawater sulfate concentrations. Biogeoscience Discussions 11, 13187–
1081 13250.

1082 Alt, J.C., 1995. Sulfur isotopic profile through the oceanic crust: sulfur mobility and seawater-
1083 crustal sulfur exchange during hydrothermal alteration. Geology 23, 585–588.

1084 Anbar, A.D., Knoll, A.H., 2002. Proterozoic ocean chemistry and evolution: A bioinorganic
1085 bridge? Science 297, 1137–1142.

1086

1087 Astini, R.A., 1995. Geologic meaning of Arenig–Llanvirn diachronous black shales
1088 (Gualcamayo Alloformation) in the Argentine Precordillera, tectonic or eustatic? Ordovician
1089 Odyssey: Short Papers for the 7th International Symposium on the Ordovician System.
1090 Pacific Section, Society for Sedimentary Geology, Fullerton, CA, pp. 217–220.

1091 Astini, R.A., Benedetto, J.L., Vaccari, N.E., 1995. The early Paleozoic evolution of the
1092 Argentine Precordillera as a Laurentian rifted, drifted, and collided terrane: a geodynamic
1093 model. Geological Society of America Bulletin 107 (3), 253–273.

1094 Astini, R.A., Collo, G., Martina, F., 2007. Ordovician K-bentonites in the upper-plate active
1095 margin of Western Gondwana, (Famatina Ranges): stratigraphic and palaeogeographic
1096 significance. Gondwana Research 11, 311–325.

1097 Azmy, K., Lavoie, D., 2009. High-resolution isotope stratigraphy of the Lower Ordovician St.
1098 George Group of western Newfoundland, Canada: implications for global correlation.
1099 Canadian Journal of Earth Sciences 46, 403–423.

1100 Azmy, K., Lavoie, D., Knight, I., Chi, G., 2008. Dolomitization of the Lower Ordovician
1101 Aguathuna Formation carbonates, Port au Port Peninsula, western Newfoundland, Canada:
1102 implications for a hydrocarbon reservoir. Canadian Journal of Earth Sciences 45, 795–813.

1103 Banner, J.L., Hanson, G.N., 1990. Calculation of simultaneous isotopic and trace element
1104 variations during water–rock interaction with applications to carbonate diagenesis.
1105 Geochimica et Cosmochimica Acta 54, 3123–3137.

1106 Bartley, J.K., Kah, L.C., Williams, J.L., Stagner, A.F., 2007. Carbon isotope chemostratigraphy
1107 of the Middle Riphean type section (Avzyan Formation, Southern Urals, Russia): signal
1108 recovery in a fold-and-thrust belt. Chemical Geology 237, 211–232.

1109 Bergström, S.M., Chen, X., Gutierrez-Marco, J.C., Dronov, A., 2008. The new
1110 chronostratigraphic classification of the Ordovician System and its relations to major
1111 regional series and stages and to $\delta^{13}C$ chemostratigraphy. Lethaia 42, 97–107.

1112 Berner, R.A., 1984. Sedimentary pyrite formation: an update. Geochimica et Cosmochimica
1113 Acta 48, 605–615.

1114 Berner, R.A., 1987. Models for carbon and sulfur cycles and atmospheric oxygen: Application to
1115 Paleozoic geologic history. American Journal of Science 287, 177–196.

1116 Berner, R.A., 1994. GEOCARB II: a revised model of atmospheric CO2 over Phanerozoic time.

American Journal of Science 294, 56–91.

Berner, R.A., Raiswell, R.A., 1983. Burial of organic-carbon and pyrite sulfur over Phanerozoic time—A new theory: Geochimica et Cosmochimica Acta 47, 855–862.

Berner, R.A., Beerling, D.J., Dudley, R., Robinson, J.M., Wildman, R.A., Jr., 2003. Phanerozoic atmospheric oxygen: Annual Review of Earth and Planetary Sciences 31, 105–134.

Bottomley, D.J., Veizer, J., Nielsen, H., Moczydlowska, M., 1992. Isotopic composition of disseminated sulfur in Precambrian sedimentary rocks. Geochimica et Cosmochimica Acta 56, 3311–3322.

Bowles, M.W., Mogollón, J.M., Kasten, S., Zabel, M., Hinrichs, K-U., 2014. Global rates of marine sulfate reduction and implications for sea-floor metabolic activities. Science 244, 889-891.

Brenchley, P., Marshall, J., Carden, G., Robertson, D., Long, D., Meidla, T., Hints, L., Anderson, T.F., 1994. Bathymetric and isotopic evidence for a short-lived Late Ordovician glaciation in a greenhouse period. Geology 22, 295–298.

Brennan, S.T., Lowenstein, T.K., Horita, J., 2004. Seawater chemistry and the advent of biocalcification. Geology 32, 473–476.

Brocks, J.J., Love, G.D., Summons, R.E., Knoll, A.H., Logan, G.A., Bowden, S.A., 2005. Biomarker evidence for green and purple sulphur bacteria in a stratified Palaeoproterozoic sea. Nature 437,866–870.

Brüchert, V., 2004. Physiological and ecological aspects of sulfur isotope fractionation during

bacterial sulfate reduction. Geological Society of America, Special Paper 379, 1-16.

Buatois, L.A., Mángano, M.G., Brussa, E.D., Benedetto, J.L., Pompei, J.F., 2009. The changing face of the deep: Colonization of the early Ordovician deep-sea floor, Puna, northwest Argentina. Palaeogeography, Palaeoclimatology, Palaeoecology 280, 291-299

Buggisch, W., Keller, M., Lehnert, O., 2003. Carbon isotope record of the Late Cambrian to Early Ordovician carbonates of the Argentine Precordillera. Palaeogeography, Palaeoclimatology, Palaeoecology 195, 357–373.

Burdett, J.W., Arthur, M.A., Richardson, M., 1989. A Neogene seawater sulfur isotope age curve from calcareous pelagic microfossils. Earth and Planetary Science Letters 94, 189–198.

Cañas, F.L., 1999. Facies and sequences of the Late Cambrian–Early Ordovician carbonates of the Argentine Precordillera: a stratigraphic comparison with Laurentian platforms. In: Ramos, V.A., Keppie, J.D. (Eds.), Laurentia–Gondwana Connections before Pangea: Geological Society of America, Special Paper, 336, pp. 43–62.

Cañas, F., Carrera, M., 1993. Early Ordovician microbial-sponge-receptaculitid bioherms of the Precordillera, western Argentina. Facies 29, 169-178.

Canfield, D.E., 2001. Biogeochemistry of sulphur isotopes. In: Valley, J.W., Cole, D.R. (Eds.), Stable Isotope Geochemistry, 607–633.

Canfield, D.E., 2005. The early history of atmospheric oxygen: Homage to Robert M. Garrels. Annual Review of Earth and Planetary Sciences 33, 1–36.

Canfield, D.E., Teske, A., 1996. Late Proterozoic rise in atmospheric oxygen concentration

1157 inferred from phylogenetic and sulphur-isotope studies. Science 382, 127–132.

1158 Canfield, D.E., Thamdrup, B., 1994. The production of ^{34}S-depleted sulphide during bacterial
1159 disproportionation of elemental sulphur. Science 266, 1973–1975.

1160 Canfield, D.E., Raiswell, R., Westrich, J.T., Reaves, C.M., Berner, R.A., 1986. The use of
1161 chromium reduction in the analysis of reduced inorganic sulfur in sediments and shales.
1162 Chemical Geology 54, 149–155.

1163 Canfield, D.E., Raiswell, R., Bottrell, S.H., 1992. The reactivity of sedimentary iron minerals
1164 toward sulfide. American Journal of Science 292, 659-683.

1165 Canfield, D.E., Farquhar, J., Zerkle, A.L., 2010. High isotope fractionations during sulfate
1166 reduction in a low-sulfate euxinic ocean analog. Geology 38, 415-418.

1167 Chen, D., Wang, J., Racki, G., Li, H., Wang, C., Ma, X., Whalen, M.T., 2013. Large sulphur
1168 isotopic perturbations and oceanic changes during the Frasnian-Famennian transition of the
1169 Late Devonian. Journal of the Geological Society of London 170, 465-476.

1170 Chen, X., Rong, J., Wang, X., Wang, Z., Zhang, Y., Zhan, R., 1995. Correlation of the
1171 Ordovician rocks of China. International Union of Geological Sciences Publication 31, 1–
1172 104.

1173 Chen, X., Rong, J., Li, Y., Boucot, A.J., 2004. Facies patterns and geography of the Yangtze
1174 region, South China, through the Ordovician and Silurian transition. Palaeogeography,
1175 Palaeoclimatology, Palaeoecology 204, 353–372.

1176 Chiba, H., Sakai, H., 1985. Oxygen isotope exchange rate between dissolved sulfate and water at

1177 hydrothermal temperatures. Geochimica et Cosmochimica Acta 49, 993–1000.

1178 Cocks, L.R.M., Torsvik, T.H., 2002. Earth geography from 500 to 400 million years ago: a
1179 faunal and palaeomagnetic review. Journal of the Geological Society of London 159, 631–
1180 644.

1181 Cocks, L.R.M., Torsvik, T.H., 2011. The Palaeozoic geography of Laurentia and western
1182 Laurussia: a stable craton with mobile margins. Earth-Science Reviews 106, 1–51.

1183 Cocks, L.R.M., Torsvik, T.H., 2013. The dynamic evolution of the Paleogeography of eastern
1184 Asia. Earth-Science Reviews 117, 40–79.

1185 Dahl, T.W., Hammarland, E.U., Anbar, A.D., Bond, D.P., Gill, B.C., Gordon, G.W., 2010.
1186 Devonian rise in atmospheric oxygen correlated to the radiations of terrestrial plants and
1187 large predatory fish. Proceedings of the National Academy of Sciences, 107, 17911–17915.

1188 Davison, W., 1982. Transport of iron and manganese in relation to the shapes of their
1189 concentration-depth profiles. Hydrobiologia 92, 463–471.

1190 Delabroye, A., Vecoli, M., 2010. The end-Ordovician glaciation and the Hirnantian Stage: a
1191 global review and questions about Late Ordovician event stratigraphy. Earth Science
1192 Reviews 98, 269–282.

1193 Derry, L.A., Kaufman, A.J., Jacobsen, S.B., 1992. Sedimentary cycling and environmental
1194 change in the Late Proterozoic: evidence from stable and radiogenic isotopes. Geochimica et
1195 Cosmochimica Acta 56, 1317–1329.

1196 Detmers, J. Brüchert, V., Habicht, K.S., Kuever, J., 2001. Diversity of sulfur isotope

1197 fractionations by sulfate-reducing prokaryotes. Applied Environmental Microbiology 67,
1198 888–894.

1199 Droser, M.L., Finnegan, S., 2003. The Ordovician radiation: a follow-up to the Cambrian
1200 explosion. Integrative and Comparative Biology 43, 178–184.

1201 Edwards, C.T., Saltzman, M.R., 2014. Carbon isotope (δ^{13}Ccarb) stratigraphy of the Lower-
1202 Middle Ordovician (Tremadocian-Darriwilian) in the Great Basin, western United States:
1203 Implications for global correlation. Palaeogeography, Palaeoclimatology, Palaeoecology 399,
1204 120.

1205 Fanning, C.M., Pankhurst, R.J., Rapela, C.W., Baldo, E.G., Casquet, C., Galindo, C., 2004. K-
1206 bentonites in the Argentine Precordillera contemporaneous with rhyolite volcanism in the
1207 Famatinian Arc. Journal of the Geological Society of London 161, 747–756.

1208 Feng, L., Li, C., Huang, J., Chang, H., Chu, X., 2014. A sulfate control on marine mid-depth
1209 euxinia on the early Cambrian (ca. 529-521 Ma) Yangtze platform, South China.
1210 Precambrian Research 246, 123-133.

1211 Fike, D.A., Grotzinger, J.P., Pratt, L.M., Summons, R.E., 2006. Oxidation of the Ediacaran
1212 Ocean. Nature 444, 744–747.

1213 Filippelli, G.M., Sierro, F.J., Flores, J.A., Vasquez, A., Utrilla, R., Perez-Folgado, M., Latimer,
1214 J.C., 2003. A sediment-nutrient-oxygen feedback responsible for productivity variations in
1215 late Miocene sapropel sequences of the western Mediterranean: Palaeogeography,
1216 Palaeoclimatology, Palaeoecology 190, 335–348.

1217 Finnegan, S., Bergman, K., Eiler, J.M., Jones, D.S., Fike, D.A., Eisenman, I., Hughes, N.C.,
1218 Tripati, A.K., Fischer,W.W., 2011. The magnitude and duration of Late Ordovician-Early
1219 Silurian glaciation. Science 331, 903–908.

1220 Frank, T.D., Lohmann, K.C., 1996. Diagenesis of fibrous magnesian calcite marine cement:
1221 implications for the interpretation of $\delta^{18}O$ and $\delta^{13}C$ values of ancient equivalents.
1222 Geochimica et Cosmochimica Acta 60, 2427–2436.

1223 Frank, T.D., Kah, L.C., Lyons, T.W., 2004. Changes in organic matter production and
1224 accumulation as a mechanism for isotopic evolution in the Mesoproterozoic ocean.
1225 Geological Magazine 140, 397–420.

1226 Fry, B., Ruf, W., Gest, H., Hayes, J.M., 1988. Sulfur isotope effects associated with oxidation of
1227 sulfide by O_2 in aqueous solution. Isotope Geoscience 73, 205–210

1228 Gill, B.C., Lyons, T.W., Saltzman, M.R., 2007. Parallel, high-resolution carbon and sulfur
1229 isotope records of the evolving Paleozoic marine sulfur reservoir. Palaeogeography,
1230 Palaeoclimatology, Palaeoecology 256, 156–173.

1231 Gill, B.C., Lyons, T.W., Frank, T.D., 2008. Behavior of carbonate-associated sulfate during
1232 meteoric diagenesis and implications for the sulfur isotope paleoproxy. Geochimica et
1233 Cosmochimica Acta 72, 4699–4711.

1234 Gill, B.C., Lyons, T.W., Young, S.A., Kump, L.R., Knoll, A.H., Saltzman, M.R., 2011.
1235 Geochemical evidence for widespread euxinia in the Late Cambrian ocean. Nature 69, 80–83.

1236 Gilleaudeau, G.J., Kah, L.C., 2013. Carbon isotope records in a Mesoproterozoic epicratonic sea:

1237 Carbon cycling in a low-oxygen world. Precambrian Research 228, 85–101.

1238 Goldberg, T., Poulton, S.W., Strauss, H., 2005. Sulphur and oxygen isotope signatures of late
1239 Neoproterozoic to early Cambrian sulphate, Yangtze Platform, China: diagenetic constraints
1240 and seawater evolution. Precambrian Research 137, 223–241.

1241 Gomes, M.L., Hurtgen, M.T., 2013. Sulfur isotope systematics of a euxinic, low-sulfate lake:
1242 evaluating the importance of the reservoir effect in modern and ancient oceans. Geology 41,
1243 663–666.

1244 Gomes, M.L., Hurtgen, M.T., 2013. Sulfur isotope fractionation in modern euxinix systems:
1245 Implications for paleoenvironmental recornstructions of paired sulfate-sulfide isotope records.
1246 Geochemica et Cosmochimica Acta 157, 39-55.

1247 Gomez, F.J., Ogle, N., Astini, R.A., Kalin, R.M., 2007. Paleoenvironmental and carbon–oxygen
1248 isotope record of Middle Cambrian carbonates (La Laja Formation) in the Argentine
1249 Precordillera. Journal of Sedimentary Research 77, 826–842.

1250 Gorjan, P., Veevers, J.J., Walter, M.R., 2000. Neoproterozoic sulfur-isotope variation in
1251 Australia and global implications. Precambrian Research 100, 151–179.

1252 Gruber, N., Sarmiento, J.L., 1997. Global patterns of marine nitrogen fixation and denitrification.
1253 Global Biogeochemical Cycles 11, 235–266.

1254 Guo, H., Du, Y., Kah, L.C., Hu, C., Huang, J., Huang, H., Yu, W., Song, H., 2015. Sulfur isotope
1255 composition of carbonate-associated sulfate from the Mesoproterozoic Jixian Group, North
1256 China: implications for the marine sulfur cycle. Precambrian Research, in press.

1257 Habicht, K.S., Canfield, D.E., 1996. Sulphur isotope fractionation in modern microbial mats and
1258 the evolution of the sulphur cycle. Nature 382, 342–343.

1259 Habicht, K.S., Canfield, D.E., 1997. Sulfur isotope fractionation during bacterial sulfate
1260 reduction in organic-rich sediments. Geochimica et Cosmochimica Acta 67, 5351–5361.

1261 Habicht, K.S., Canfield, D.E., 2001. Isotope fractionation by sulfate-reducing natural populations
1262 and the isotopic composition of sulfide in marine sediments. Geology 29, 555–558.

1263 Habicht, K.S., Canfield, D.E., Rethmeier, J., 1998. Sulfur isotope fractionation during bacterial
1264 reduction and disproportionation of thiosulfate and sulfite. Geochimica et Cosmochimica
1265 Acta 62, 2585–2595.

1266 Hannigan, R., Brookfield, M.E., Basu, A.R., 2010. A detailed 87Sr/86Sr isotope curve for the
1267 mid-Cincinnnatian (Upper Katian–Lower Hirnantian, Upper Ordovician), NE North
1268 American shelf (Ontario, Canada). Chemical Geology 277, 336–344.

1269 Haq, B.U., Schutter, S.R., 2008. A chronology of Paleozoic sea-level changes. Science 322, 64–
1270 68.

1271 Harper, D.A.T., Hammarlund, E.U., Rasmussen, C.M.Ø., 2013. End Ordovician Extinctions:
1272 ACoincidence of Causes. Gondwana Research 25, 1294–1307.

1273 Harper, D.A.T., MacNiocaill, C., Williams, S.H., 1996. The palaeogeography of early
1274 Ordovician Iapetus terranes: an integration of faunal and palaeomagnetic constraints.
1275 Palaeogeography, Palaeoclimatology, Palaeoecology 121, 297–312.

1276 Harrison, A.G., Thode, H.G., 1957. The kinetic isotope effect in the chemical reduction of

1277 sulphate. Transactions of the Faraday Society 53, 1648–1651.

1278 Hayes, J.M., Lambert, I.B., Strauss, H., 1992. The sulfur-isotopic record, in J.W. Schopf and C.
1279 Klein, eds., The Proterozoic Biosphere: A Multidisciplinary Study: Cambridge, Cambridge
1280 University Press, 129–131.

1281 Higgins, J.A., Fischer, W.W., Schrag, D.P., 2009. Oxygenation of the ocean and sediments:
1282 consequences for the seafloor carbonate factory. Earth and Planetary Science Letters 284,
1283 25–33.

1284 Hints, O., Martma, T., Männik, P., Nolvak, J., Poldvere, A., Shen, Y., Virra, V., 2014. New data
1285 on Ordovician stable isotope record and conodont biostratigraphy from the Viki reference
1286 drill core, Saaremaa Isaland, western Estonia. GFF 136, 100-104.

1287 Holser, W.T., Schidlowski, M., Mackenzie, F.T., Maynard, J.B., 1988. Geochemical cycles of
1288 carbon and sulfur. In: Gregor, C.B., Garrels, R.M., Mackenzie, F.T., Maynard, J.B. (Eds.),
1289 Chemical Cycles in the Evolution of the Earth.Wiley, New York, 105–173.

1290 Horita, J., Zimmermann, H., Holland, H.D., 2002. Chemical evolution of seawater during the
1291 Phanerozoic: implications from the record of marine evaporites. Geochimica et
1292 Cosmochimica Acta 66, 3733–3756.

1293 Hough, M.L., Shields, G.A., Evins, L.Z., Strauss, H., Mackenzie, S., 2006. A major sulphur
1294 isotope event at **c**. 510 Ma: a possible anoxic–extinction–volcanism connection during the
1295 Early–Middle Cambrian transition? Terra Nova 18, 257–263.

1296 Huff, W.D., Davis, D., Bergström, S.M., Krekeler, M.P.S., Kolata, D.R., Cingolani, C., 1997. A

biostratigraphically well-constrained K-bentonite U–Pb zircon age of the lowermost Darriwilian State (Middle Ordovician) from the Argentine Precordillera. Episodes 20, 29–33.

Hurtgen, M., Arthur, M., Suits, N., Kaufman, A., 2002. The sulfur isotopic composition of Neoproterozoic seawater sulfate: implications for snowball Earth? Earth and Planetary Science Letters 203, 413–429.

Hurtgen, M.T., Arthur, M.A., Halverson, G.P., 2005. Neoproterozoic sulfur isotopes, the evolution of microbial sulfur species, and the burial efficiency of sulfide as sedimentary sulfide. Geology 33, 41–44.

Hurtgen, M.T., Pruss, S.B., Knoll, A.H., 2009. Evaluating the relationship between the carbon and sulfur cycles in the later Cambrian ocean: an example from the Port au Port Group, western Newfoundland, Canada. Earth and Planetary Science Letters 281, 288–297.

James, N.P., Barnes, C.R., Stevens, R.K., Knight, I., 1989. A lower Paleozoic continental margin carbonate platform, northern Canadian Appalachians. In: Crevello, T., Sarg, R., Read, J.F., Wilson, J.L. (Eds.), Controls on carbonate platforms and basin development: Society of Economic Paleontologists and Mineralogists, Special Publications, 44, pp. 123–146.

Jones, D.S., Fike, D.A., 2013. Dynamic sulfur and carbon cycling through the end-Ordovician extinction revealed by paired sulfate-pyrite d34S. Earth and Planetary Science Letters 363, 144–155.

Jørgensen, B.B., Bang, M., Blackburn, T.H., 1990. Anaerobic mineralization in marine sediments from the Baltic Sea–North Sea transition. Marine Ecology Progress Series 59, 39–54.

1318 Kah, L.C., Sherman, A.B., Narbonne, G.M., Kaufman, A.J., Knoll, A.H., 1999. δ13C
1319 stratigraphy of the Proterozoic Bylot Supergroup, northern Baffin Island: implications for
1320 regional lithostratigraphic correlations. Canadian Journal of Earth Sciences 36, 313–332.

1321 Kah, L.C., Lyons, T.W., Chesley, J.T., 2001. Geochemistry of a 1.2 Ga carbonate-evaporite
1322 succession, northern Baffin and Bylot Islands: implications for Mesoproterozoic marine
1323 evolution. Precambrian Research 111, 203–234.

1324 Kah, L.C., Lyons, T.W., Frank, T.D., 2004. Low marine sulphate and protracted oxygenation of
1325 the Proterozoic biosphere. Nature 431, 834–838.

1326 Kah, L.C., Bartley, J.K., and Teal, D.A., 2012. Chemostratigraphy of the late Mesoproterozoic
1327 Atar Group, Mauritania: Muted isotopic variability, facies correlation, and global isotopic
1328 trends. Precambrian Research 200-203, 82–103.

1329 Kaljo, D., Martma, T., Saadre, T., 2007. Post-Hunnebergian Ordovician carbon isotope trend in
1330 Baltoscanadia, its environmental implications and some similarities with that of Nevada.
1331 Palaeogeography, Palaeoclimatology, Palaeoecology 245, 138–155.

1332 Kampschulte, A., Bruckschen, P., Strauss, H., 2001. The sulphur isotopic composition of trace
1333 sulphates in Carboniferous brachiopods: implications for coeval seawater correlation with
1334 other geochemical cycles and isotope stratigraphy. Chemical Geology 175, 149–173.

1335 Kaplan, I.R., Rittenberg, S.C., 1964. Microbiological fractionation of sulphur isotopes. Journal
1336 of General Microbiology 34, 195–212.

1337 Kaufman, A.J., Knoll, A.H., 1995. Neoproterozoic variations in the C-isotopic composition of

1338 seawater: stratigraphic and biogeochemical implications. Precamrbian Research 73, 27–49.

1339 Keppie, J.D., Keppie, D.F., 2014. Ediacaran–Middle Paleozoic oceanic voyage of Avalonia from
1340 Baltica via Gondwana to Laurentia: Paleomagnetic, faunal and geological constraints.
1341 Geoscience Canada 41.

1342 Kitano, Y., Okumura, M., Idogake, M., 1985. Incorporation of sodium, chloride and sulfate with
1343 calcium carbonate. Geochemistry Journal 9, 75–84.

1344 Klappa, C.F., Opalinski, P.R., James, N.P., 1980. Middle Ordovician Table Head Group of
1345 western Newfoundland: a revised stratigraphy. Canadian Journal of Earth Sciences 17, 1007–
1346 1019.

1347 Knoll, A.H., Carroll, S.B., 1999. Early animal evolution: Emerging views from comparative
1348 biology and geology. Science 284, 2130–2137.

1349 Kump, L.R., Arthur, M.A., 1999. Interpreting carbon-isotope excursions: Carbonates and organic
1350 matter. Chemical Geology 161, 181–198.

1351 Kump, L.R., 1989. Alternative modeling approaches to the geochemical cycles of carbon, sulfur,
1352 and strontium isotopes. American Journal of Science 289, 390–410.

1353 Kurtz, A.C., Kump, L.R., Arthur, M.A., Zachos, J.C., Paytan, A., 2003. Early Cenozoic
1354 decoupling of the global carbon and sulfur cycles. Paleoceanography, 18,
1355 http://dx.doi.org/10.1029/2003PA000908.

1356 Lavoie, D., Burden, E., Lebel, D., 2003. Stratigraphic framework for the Cambrian-Ordovician
1357 rift and passive margin successions from southern Quebec to western Newfoundland.

1358 Canadian Journal of Earth Sciences 40, 177–205.

1359 Lefebvre, V., Sarvais, T., Francois, L., Averbuch, O., 2010. Did a Katian large igneous province
1360 trigger the Late Ordovician glaciation? A hypothesis tested with a carbon cycle model.
1361 Palaeogeography, Palaeoclimatology, Palaeoecology 296, 310–319.

1362 Lenton, T.M., Watson, A.J., 2000. Redfield revisited 1. Regulation of nitrate, phosphate, and
1363 oxygen in the ocean: Global Biogeochemical Cycles 14, 225–248.

1364 Li, R., Chen, J., Zhang, S., Lei, J., Shen, Y., Chen, X., 1999. Spatial and temporal variations in
1365 carbon and sulfur isotopic compositions of Sinian sedimentary rocks in the Yangtze platform,
1366 South China. Precambrian Research 97, 59–75.

1367 Li, C., Love, G.D., Lyons, T.W., Fike, D.A., Sessions, A.L., Chu, X., 2010. A stratified redox
1368 model for the Ediacaran Ocean. Science 328, 80–83.

1369 Lowenstein, T.K., Timofeeff, M.N., Brennan, S.T., Hardie, L.A., Demicco, R.V., 2001.
1370 Oscillations in Phanerozoic seawater chemistry: evidence from fluid inclusions. Science 294,
1371 1086–1088.

1372 Lowenstein, T.K., Hardie, L.A., Timofeeff,M.N., Demicco, R.M., 2003. Secular variation in
1373 seawater chemistry and the origin of calcium chloride basinal brines. Geology 31, 857–860.

1374 Luo, G.M., Junium, C.K., Kump, L.R., Huang, J.H., Li, C., Feng, Q.L., Shi, X.Y., Bai, X., Xie,
1375 S.C., 2014a. Shallow stratification prevailed for ~1700 to ~1300 Ma ocean: evidence from
1376 organic carbon isotope composition in the North China Block. Earth and Planetary Science
1377 Letters 400, 219-232.

1378 Luo, G., Ono, S., Huang, J., Algeo, T.J., Li, C., Zhou, L., Robinson, A., Lyons, T.W., Xie, S.,
1379 2015b. Decline in oceanic sulfate levels during the early Mesoproterozoic. Precambrian
1380 Research 258, 36–47.

1381 Lyons, T.W., 2004. Sites of anomalous organic remineralization in the carbonate sediments of
1382 South Florida, USA: the sulfur cycle and carbonate-associated sulfate. Geological Society of
1383 America Special Paper 379, 161–176.

1384 Lyons, T.W., Severmann, S., 2006. A critical look at iron paleoredox proxies based on new
1385 insights from modern euxinic marine basins. Geochimica et Cosmochimica Acta 70, 5698–
1386 5722.

1387 Lyons, T.W., Anbar, A.D., Severmann, S., Scott, C., Gill, B.C., 2009. Tracking euxinia in the
1388 ancient ocean: a multiproxy case study. Annual Reviews of Earth and Planetary Sciences 37,
1389 506–534.

1390 MacNiociall, C., van der Pluijm, B., Van der Voo, R., 1997. Ordovician Paleogeography and the
1391 evolution of the Iapetus ocean. Geology 25, 159–162.

1392 Männik, P., Viira, V., 2005. Distribution of conodonts. In Mehikoorma (421) Drill Core.
1393 Estonian Geological Sections 6, 16–20.

1394 Marenco, P.J., Corsetti, F.A., Hammond, D.E., Kaufman, A.J., Bottjer, D.J., 2008. Oxidation of
1395 pyrite during extraction of carbonate associated sulfate. Chemical Geology 247, 124–132.

1396 Marenco, P.J., Marenco, K.N., Lubitz, R.L., Niu, D., 2013. Contrasting long-term global and
1397 short-term local redox proxies during the Great Ordovician Biodiversification Event: A case

study from Fossil Mountain, Utah, USA. Palaeogeography, Palaeoclimatology, Palaeoecology 377, 45-51.

Mazmudar, A., Goldberg, T., Strauss, H., 2008. Abitic oxidation of pyrite by Fe(III) in acidic media and its implications for sulfur isotope measurements of lattice bound sulfate in sediments. Chemical Geology 253, 30–37.

McFadden, K.A., Huang, J., Chu, X., Jiang, G., Kaufman, A.J., Zhou, C., Yuan, X., Xiao, S., 2008. Pulsed oxidation and biological evolution in the Ediacaran Doushantuo Formation. Proceedings of the National Academy of Sciences 105, 3197–3202.

Meyer, K.M., Kump, L.R., 2008. Ocean Euxinia in earth history: causes and consequences. Annual Review of Earth and Planetary Science 36, 251–288.

Miller, K.G., Kominz, M.A., Browning, J.V., Wright, J.D., Mountain, G.S., Katz, M.E., Sugarman, P.J., Cramer, B.S., Christie-Blick, N., Pekar, S.F., 2005. The Phanerozoic record of global sea-level change. Science 310, 1293–1298.

Miller, A.I., 1997. Dissecting global diversity trends: examples from the Ordovician radiation. Annual Review of Ecology and Systematics 28, 85–104.

Montanez, I.P., Banner, J.L., Osleger, D.A., Borg, L.E., Bosserman, P.J., 1996. Integrated Sr isotope variations and sea-level history of Middle to Upper Cambrian platform carbonates: Implications for the evolution of Cambrian seawater $^{87}Sr/^{86}Sr$. Geology 24, 917-920.

Munnecke, A., Calner, M., Harper, D.A.T., Servais, T., 2010. Ordovician and Silurian seawater chemistry, sea level, and climate: a synopsis. Palaeogeography, Palaeoclimatology,

1418 Palaeoecology 296, 389–413.

1419 Munnecke, A., Zhange, Y., Liu, Z., Cheng, J., 2011. Stable carbon isotope stratigraphy in the
1420 Ordovician of South China. Palaeogeography, Palaeoclimatology, Palaeoecology 307, 17-43.

1421 Murphy, J.B., Keppie, J.D., Nance, R.D., Dostal, J., 2010. Comparative evolution of the Iapetus
1422 and Rheic oceans: a Northa America perspective. Gondwana Research 17, 482–499.

1423 Nance, R.D., Gutierrez-Alonso, G., Keppie, J.D., Linnemann, U., Murphy, J.B., Quesada, C.,
1424 Strachan, R.A., Woodcock, N.H., 2012. A brief history of the Rheic ocean. Geoscience
1425 Frontiers 3, 125-135.

1426 Okouchi, N., Kawamura, K., Kajiwara, Y., Wada, E., Okada, M., Kanamatsu, T., Taira, A., 1999.
1427 Sulfur isotope records around Livello Bonarelli (northern Apennines, Italy) black shale at the
1428 Cenomanian-Turonian boundary. Geology 27, 535-538.

1429 Owens, J.D., Gill, B.C., Jenkyns, H.C., Bates, S.M., Severmann, S., Kuypers, M.M.M.,
1430 Woodfine, R.G., Lyons, T.W., 2013. Sulur isotopes track the global extent and dynamics of
1431 euxinia during Cretaceous Oceanic Anoxic Event 2. Proceedings of the National Academy of
1432 Sciences 110, 18407-18412.

1433 Petrychenko, O.Y., Peryt, T.M., Chechel, E.I., 2005. Early Cambrian seawater chemistry from
1434 fluid inclusions in halite from Siberian evaporites. Chemican Geology 219, 149–161.

1435 Paytan, A., Kastner, M., Campbell, D., Thiemens, M.H., 1998. Sulfur isotopic composition of
1436 Cenozoic seawater sulfate. Science 282, 1459–1462.

1437 Paytan, A., Mearon, S., Cobb, K., Kastner, M., 2002. Origin of marine barite deposits: Sr and S

1438 isotope characterization. Geology 30, 747-750.

1439 Petsch, S.T., Berner, R.A., 1998. Coupling the long-term geochemical cycles of carbon,
1440 phosphorus, sulfur, and iron: the effect on atmospheric O2 and the isotopic records of carbon
1441 and sulfur. American Journal of Science 298, 246–262.

1442 Pope, M.C., Steffen, J.B., 2003. Widespread, prolonged late Middle to Late Ordovician
1443 upwelling in North America: a proxy record of glaciation? Geology 31, 63–66.

1444 Poulton, S.W., Fralick, P.W., Canfield, D.E., 2004. The transition to a sulphidic ocean 1.84
1445 billion years ago. Nature 431, 173–177.

1446 Present, T.M., Paris, G., Burke, A., Fischer, W.W., Adkins, J.F., 2015. Large Carbonate-
1447 associated sulfate isotopic variability between brachiopods, micrite, and other sedimentary
1448 components in Late Ordovician strata. Earth and Planetary Science Letters 432, 187–198.

1449 Qing, H., Veizer, J., 1994. Oxygen and carbon isotopic composition of Ordovician brachiopods:
1450 implications for coeval seawater. Geochimica et Cosmochimica Acta 58, 4429–4442.

1451 Qing, H., Barnes, C.R., Buhl, D., Veizer, J., 1998. The strontium isotopic composition of
1452 Ordovician and Silurian brachiopods and conodonts: relationships to geological events and
1453 implications for coeval seawater. Geochimica et Cosmochimica Acta 62, 1721–1733.

1454 Quinton, P.C., MacLeod, K.G., 2014. Oxygen isotopes from conodont apatite of the
1455 midcontinents, US: Implications for Late Ordovician climate evolution. Palaeogeography,
1456 Palaeoclimatology, Palaeoecology 404, 57–66.

1457 Raab, M., Spiro, B., 1991. Sulfur isotopic variations during seawater evaporation with fractional
1458 crystallization. Chemical Geology. Isotope Geoscience Section 86, 323–333.

1459 Raiswell, R., Berner, R.A., 1985. Pyrite formation in euxinic and semi-euxinic sediments.
1460 American Journal of Science 285, 710-724.

1461 Rennie, V.C.F., Turchyn, A.V., 2014. The preservation of $\delta^{34}S_{SO4}$ and $\delta^{18}O_{SO4}$ in carbonate-
1462 associated sulfate during marine diagenesis: a 25 Myr test case using marine sediments. Earth
1463 and Planetary Science Letters 395, 13-23.

1464 Rasmussen, C.M.Ø., Harper, D.A.T., 2008. Resolving early Mid-Ordovician (Kundian)
1465 bioevents in the East Baltic based on brachiopods. Geobios 41, 533–542.

1466 Reinhard, C.T., Planavsky, N.J., Robbins, L.J., Partin, C.A., Gill, B.C., Lalonde, S.V., 2013.
1467 Proterozoic ocean redox and biogeochemical stasis. Proceedings of the National Academy of
1468 Sciences, 110, 5357–5362.

1469 Ries, J.B., Fike, D.A., Pratt, L.M., Lyons, T.W., Grotzinger, J.P., 2009. Superheavy pyrite in the
1470 terminal Proterozoic Nama Group, southern Namibia: a consequence of low seawater sulfate
1471 at the dawn of animal life. Geology 37, 743–746.

1472 Rothman, D.H., Hayes, J.M., Summons, R.E., 2003. Dynamics of the Neoproterozoic carbon
1473 cycle. Proceedings of the National Academy of Sciences 100, 8124–8129.

1474 Sælen, G., Raiswell, R., Talbot, M.R., Skei, J.M., Bottrell, S.H., 1993. Heavy sedimentary sulfur
1475 isotopes as indicators of super-anoxic bottom-water conditions. Geology, 21, 1091–1094.

1476 Saltzman, M.R., 2005. Phosphorus, nitrogen, and the redox evolution of the Paleozoic oceans.

1477 Geology 33, 573–576.

1478 Saltzman, M.R., Young, S.A., 2005. Long-lived glaciation in the Late Ordovician? Isotopic and
1479 sequence-stratigraphic evidence from western Laurentia. Geology 33, 109–112.

1480 Sarmiento, J.L., Herbert, T., Toggweiler, J.R., 1988. Causes of anoxia in the world ocean. Global
1481 Biogeochemical Cycles 2, 115–128.

1482 Schmitz, B., Bergstrom, S.M., 2007. Chemostratigraphy in the Swedish Upper Ordovician:
1483 Regional significance of the Hirnantian $\delta^{13}C$ excursion (HICE) in the Boda Limestone of the
1484 Siljan region. GFF 129, 133–140.

1485 Schmitz, B., Bergström, S.M., Xiaofeng, W., 2010. The middle Darriwilian (Ordovician) $\delta^{13}C$
1486 excursion (MDICE) discovered in the Yangtze Platform succession in China: implications of
1487 its first recorded occurrences outside Baltoscanadia. Journal of the Geological Society of
1488 London 167, 249–259.

1489 Scott C., Lyons T.W., 2005. Defining a uniquely euxinic molybdenum signal. Geochimica et
1490 Cosmochimica Acta 69, A577.

1491 Scott, C., Lyons, T.W., Bekker, A., Shen, Y., Poulton, S.W., Chu, X., Anbar, A.D., 2008.
1492 Tracing the stepwise oxygenation of the Proterozoic ocean. Nature 452, 456–459.

1493 Servais, T., Lehnert, O., Li, J.,Mullins, G.L., Munnecke, A., Nützel, A., Vecoli, M., 2008. The
1494 Ordovician biodiversification: revolution in the oceanic trophic chain. Lethaia 41, 99–109.

1495 Servais, T., Owen, A.W., Harper, D.A.T., Kröger, B., Munnecke, A., 2010. The Great
1496 Ordovician Biodiversification Event (GOBE): the palaeoecological dimension.

1497 Palaeogeography, Palaeoclimatology, Palaeoecology 294, 99–119.

1498 Sheehan, P.M., 2001. The Late Ordovician mass extinction. Annual Reviews of Earth and
1499 Planetary Science 29, 331–364.

1500 Shen, Y., Canfield, D.E., Knoll, A.H., 2002. Middle Proterozoic ocean chemistry: Evidence from
1501 the McArthur Basin, northern Australia. American Journal of Science 302, 81–109.

1502 Shen, B., Xiao, S., Kaufman, A.J., Bao, H., Zhou, C., Wang, H., 2008. Stratification and mixing
1503 of a post-glacial Neoproterozoic ocean: Evidence from carbon and sulfur isotopes in a cap
1504 dolostone from northwest China. Earth and Planetary Science Letters 265, 209–228.

1505 Shields, G.A., Carden, G.A.F., Veizer, J., Meidla, T., Rong, J.Y., Rong, Y.L., 2003. Sr, C, and O
1506 isotope geochemistry of Ordovician brachiopods: a major isotopic event around the Middle–
1507 Late Ordovician transition. Geochimica et Cosmochimica Acta 67, 2005–2025.

1508 Sial, A.N., Peralta, S., Gaucher, C., Toselli, A.J., Ferreira, V.P., Frei, R., Parada, M.A., Pimentel,
1509 M.M., Pereira, N.S., 2013. High-resolution stable isotope stratigraphy of the upper Cambrian
1510 and Ordovician in the Argentine Precordillera: Carbon isotope excursions and correlations.
1511 Gondwana Research 24, 330-348.

1512 Sim, M.S., Bosak, T., Ono, S., 2011. Large sulfur isotope fractionation does not require
1513 disproportionation. Science 333, 74-77.

1514 Sim, M.S., Ono, S., Hurtgen, M.T., 2015. Sulfur isotope evidence for low and fluctuating sulfate
1515 levels in the Late Devonian ocean and the potential link with the Mass extinction event. Earth
1516 and Planetary Science Letters 419, 52-62.

1517 Spear, N., Holland, H.D., Garcia-Veígas, J., Lowenstein, T.K., Giegenack, R., Peters, H., 2014.
1518 Analysis of fluid inclusions in Neoproterozoic marine halite provide oldest measurement of
1519 seawater chemistry. Geology 42, 103-106.

1520 Stenzel, S.R., James, N.P., 1987. Death and destruction of an early Paleozoic carbonate platform,
1521 western Newfoundland [abstract]. Society of Economic Paleontologists and Mineralogists,
1522 Annual Midyear Meeting, p. 80. Abstract 4.

1523 Stenzel, S.R., Knight, I., James, N.P., 1990. Carbonate platform to foreland basin: revised
1524 stratigraphy of the Table Head Group (Middle Ordovician), western Newfoundland.
1525 Canadian Journal of Earth Sciences 26, 14–26.

1526 Strauss, H., 1997. The isotopic composition of sedimentary sulfur through time.
1527 Palaeogeography, Palaeoclimatology, Palaeocology 132, 97–118.

1528 Strauss, H., 1999. Geologic evolution from isotope proxy signals—sulphur. Chemical Geology
1529 161, 89–101.

1530 Strauss, H., Bengtson, S., Myrow, P.M., Vidal, G., 1992. Stable isotope geochemistry and
1531 palynology of the Late Precambrian to Early Cambrian sequence in Newfoundland. Canadian
1532 Journal of Earth Sciences 29, 1662–1673.

1533 Takano B., 1985. Geochemical implications of sulphate in sedimentary carbonates. Chemical
1534 Geolgoy 49, 393–403.

1535 Thode, H.G., Dunford, H.B., Shima, M., 1962. Sulfur isotope abundances in rocks of the
1536 Sudbury District and their geological significance. Economic Geology 57, 565–578.

1537 Thomas, W.A., Astini, R.A., 1996. The Argentine precordillera: a traveler from the Ouachita
1538 Embayment of North America from Laurentia. Science 273, 752–757.

1539 Thomas, W.A., Astini, R.A., 1999. Simple-shear conjugate rift margins of the Argentine
1540 Precordillera and the Ouachita embayment of Laurentia. Geological Society of America
1541 Bulletin 111, 1069–1079.

1542 Thomas, W.A., Astini, R.A., 2003. Ordovician accretion of the Argentine Precordillera terrane to
1543 Gondwana: a review. Journal of South America Earth Science 16, 667–679.

1544 Thompson, C.K., Kah, L.C., 2012. Sulfur isotope evidence for widespread euxinia and a
1545 fluctuating oxycline in Early to Middle Ordovician greenhouse oceans. Palaeogeography,
1546 Palaeoclimatology, Palaeoecology 313–314, 189–214.

1547 Thompson, C.K., Kah, L.C., Astini, R., Bowring, S.A., Buchwaldt, R., 2012. Bentonite
1548 geochronology, marine geochemistry, and the Great Ordovician Biodiversification Event
1549 (GOBE). Palaeogeography, Palaeoclimatology, Palaeoecology 321–322, 88–101.

1550 Tie-bing, L., Maynard, J.B., Alten, J., 2006. Superheavy S isotopes from glacier associated
1551 sediments of the Neoproterozoic of south China: Oceanic anoxia or sulfate limitation? in S. E.
1552 Kesler and H. Ohmoto, eds., Evolution of Earth's Early Atmosphere, Hydrosphere, and
1553 Biosphere - Constraints from Ore Deposits: Geological Society of America, 205-222.

1554 Tobin, K.J., Bergstrom, S.M., De La Garza, P., 2005. A mid-Caradocian (453 Ma) drawdown in
1555 atmospgeric pCO_2 without ice sheet development? Palaeogeography, Palaeoclimatology,
1556 Palaeoecology 226, 187-204.

1557 Torres, M.E., Bohrmann, G., Dubé, T.E., Poole, F.G., 2003. Formation of modern and Paleozoic
1558 stratiform barite and cold methane seeps on continental margins. Geology 31, 897-900.

1559 Torsvik, T.H., Cocks, L.R.M., 2009. The Lower Palaeozoic palaeogeographical evolution of the
1560 northeastern and eastern peri-Gondwanan margin from Turkey to New Zealand. Geological
1561 Society, London, Special Publications 325, 3–21.

1562 Torsvik, T.H., Cocks, L.R.M., 2013. New global palaeogeographical reconstructions for the
1563 Lower Palaeozoic and their generation. Geological Society, London, Memoirs 38, 5-24.

1564 Trotter, J.A., Williams, I.S., Barnes, C.R., Lecuyer, C., Nicoll, R.S., 2008. Did cooling oceans
1565 trigger Ordovician biodiversification? Evidence from conodont thermometry. Science 321,
1566 550–554.

1567 Turchyn, A.V., Schrag, D.P., 2004. Oxygen isotope constraints on the sulfur cycle over the past
1568 10 million years. Nature 303, 2004–2007.

1569 Van Cappellen, P., Ingall, E.D., 1994. Benthic phosphorus regeneration, net primary production,
1570 and ocean anoxia: A model of the coupled marine biogeochemical cycles of carbon and
1571 phosphorus. Paleoceanography 9, 677–692.

1572 Van Staal, C.R., Barr, S.M., Murphy, J.B., 2012. Provenance and tectonic evolution of Ganderia:
1573 Constraints on the evolution of the Iapetus and Rheic oceans. Geology 40, 987–990.

1574 Veizer, J., Ala, D., Azmy, K., Bruckschen, P., Buhl, D., Bruhn, F., Carden, G.A.F., Diener, A.,
1575 Ebneth, S., Godderis, Y., Jasper, T., Korte, C., Pawellek, F., Podlaha, O.G., Strauss, H. 1999.
1576 $^{87}Sr/^{86}Sr$, $\delta^{13}C$ and $\delta^{18}O$ evolution of Phanerozoic seawater. Chemical Geology 161, 59–88.

1577 Wadleigh, M.A., Veizer, J., 1992. $^{18}O/^{16}O$ and $^{13}C/^{12}C$ in lower Paleozoic brachiopods:
1578 implications for the isotopic composition of sea water. Geochimica et Cosmochimica Acta 56,
1579 431–443.

1580 Webby, B.D., Paris, F., Droser, M.L., Percival, I.G., 2004. The Great Ordovician
1581 Biodiversification Event. Columbia University Press, New York, 1–484.

1582 Wille, M., Nägler, T.F., Lehmann, B., Schröder, S., Kramers, J.D., 2008. Hydrogen sulphide
1583 release to surface waters at the Precambrian/Cambrian boundary. Nature 453, 767–769.

1584 Williams, H., Boyce, W.D., James, N.P., 1987. Graptolites from the Lower-Middle Ordovician
1585 St. George and Table Head groups, western Newfoundland, and their correlation with
1586 trilobite, brachiopod, and conodont zones. Canadian Journal of Earth Sciences 24, 456–470.

1587 Wotte, T., Strauss, H., Fugmann, A., Garbe-Schönberg, D., 2012. Paired $\delta^{34}S$ from carbonate-
1588 associated sulfate and chromium-reducible sulfur across the traditional Lower-Middle
1589 Cambrian boundary of W-Gondwana. Geochimica et Cosmochimica Acta 85, 228-253.

1590 Xu, X., Huang, H., Liu, B., 1990. Manganese deposits of the Proterozoic Datangpo Formation,
1591 South China: genesis and palaeogeography, in J. Parnell, L. J. Ye and C. M. Chen, eds.,
1592 Sediment-hosted Mineral Deposits: Boston, Blackwell Scientific, 39-50.

1593 Yan, D., Chen, D., Wang, Q., Wang, J., 2012. Predominance of stratified anoxic Yangtze Sea
1594 interrupted by short-term oxygenation during the Ordo-Silurian transition. Chemical Geology
1595 291, 69-78.

1596 Young, S.A., Saltzman, M.R., Bergström, S.M., 2005. Upper Ordovician (Mohawkian) carbon

isotope ($\delta^{13}C$) stratigraphy in eastern and central North America: regional expression of a perturbation of the global carbon cycle. Palaeogeography, Palaeoclimatology, Palaeoecology 222, 53–76.

Young, S.A., Saltzman, M.R., Bergström, S.M., Leslie, S.A., Chen, X., 2008. Paired $\delta^{13}C$carb and $\delta^{13}C$org records of Upper Ordovician (Sandbian–Katian) carbonates in North America and China: implications for paleoceanographic change. Palaeogeography, Palaeoclimatology, Palaeoecology 270, 166–178.

Young, S.A., Saltzman, M.R., Ausich, W.I., Desrochers, A., Kaljo, D., 2010. Did changes in atmospheric CO_2 coincide with latest Ordovician glacial-interglacial cycles? Palaeogeography, Palaeoclimatology, Palaeoecology 296, 376–388.

Zhan, Renbin, Jin, Jisuo, 2007. Ordovician–Early Silurian (Llandovery) Stratigraphy and Palaeontology of the Upper Yangtze Platform. Science Press, Beijing, South China. 169 pp.

Zhan, R., Jin, J., 2008. Aspects of recent advances in the Ordovician stratigraphy and palaeontology of China. Paleoworld 17, 1–11.

Zhan, R., Jin, J., Chen, P., 2007. Brachiopod diversification during the Early-Middle Ordovician: an example from Dawan Formation, Yichang, central China. Canadian Journal of Earth Sciences 44, 9–24.

Zhang, Y., Chen, X., 2003. The Early Ordovician graptolite sequence of the Upper Yangtze region, South China. INSUGEO Serie Correlacion Geologia 17, 173–180.

Zhang, T., Shen, Y., Algeo, T.J., 2010. High-resolution carbon isotopic records from the

Ordovician of South China: links to climatic cooling and the Great Ordovician Biodiversification Event (GOBE). Palaeogeography, Palaeoclimatology, Palaeoecology 289, 102–112.

Zhou, L., Algeo, T.J., Shen, J., Hu, Z.F., Hongmei, G., Xie, S., Huang, J.H., Shan, G., 2015. Changes in marine productivity and redoc conditions during the Late Ordovician Hirnantian glaciation. Palaeogeography, Palaeoclimatology, Palaeoecology 420, 223-234.

Figure Captions

Figure 1. Single-reservoir model for sulfur cycling in marine systems. In a single-reservoir model, marine sulfate represents the primary reservoir for sulfur in the oceans. The concentration ($[SO_4^{=}]$) and the isotopic composition (δ_{SO4}) of this reservoir is determined by the relative size and isotopic composition of crustal weathering inputs (F_W, δ_W), as well as output via deposition of sedimentary sulfur as gypsum (F_{GYP}, δ_{GYP}), carbonate-associated sulfate (F_{CAS}, δ_{CAS}), or pyrite (F_{PY}, δ_{PY}), and steady state is defined as $F_W=F_{GYP+CAS}+F_{PY}$.

Figure 2. Paleogeographic context of Ordovician sample localities. Paleogeographic reconstruction after Cocks and Torsvik (2002) for the Middle Ordovician (~470 Ma). Sample localities include the Argentine Precordillera (A), Western Newfoundland (B), and the Yichang region of the South China craton (C). Location of the Precordillera is approximate and shown prior to docking with the Famatina terrain of Gondwana. Major landmasses are illustrated in white; perigondwanan terrains are illustrated in grey.

Figure 3. Location maps for Ordovician sample localities. (A) Precordilleran strata of Argentina are preserved a series of N-S trending thrust slices and comprise Eastern and Western tectofacies. Measured sections of the Ordovician San Juan, Las Chacritas, Las Aguaditas, and Gualcamayo formations were sampled within the predominantly unmetamorphosed and little deformed Eastern tectofacies. (B) Lower Paleozoic strata crop out along the western coast of Newfoundland, where they unconformably overlie Proterozoic basement of the Humber Terrain and are overlain by allochthonous sedimentary rocks associated with emplacement of the Bay of Islands ophiolite complex. Ordovician strata of the Table Head Group (Table Point and Table Cove formations) were sampled from the type section at Table Point. (C) The South China plate preserves a broadly southward deepening succession of Lower Paleozoic strata. Ordovician strata of the Huanhuayuan, Dawan, and Kuniutan formations were sampled at the Huanghuachang and Chenjiahe sections, north of Yichang.

Figure 4. Stratigraphy of Ordovician sections sampled for this study. Composite stratigraphic sections portray generalized lithologies. Argentina and western Newfoundland are drafted at identical scales, but the highly condensed section in South China has been expanded for visibility. Dashed lines represent approximate correlation tie points based on carbon isotope stratigraphy (see Fig. 6).

Figure 5. Representative facies of Ordovician strata sampled for this study. (A) Interbedded carbonate and shale of the Las Chacritas Formation, Argentina. Carbonate strata are composed primarily of sparse to packed biomicrite (B). (C) Nodular carbonate of the Table Point Formation, western Newfoundland. Strata are composed primarily of micrite, intraclastic micrite, and sparse

1662 to packed biomicrite (D), with minor secondary intergranular dolomite. (E) Clayey carbonate of
1663 the Dawan Formation, South China. Carbonate strata are represented primarily by sparse to
1664 packed biomicrite (F). All biomicrite facies show superb microfabric preservation of
1665 echinoderms, trilobites, and brachiopods.
1666
1667 **Figure 6.** Chemostratigraphic correlation of Ordovician strata from Argentina, Newfoundland,
1668 and China. The peak of a prominent, late Dapingian negative excursion is constrained to have
1669 occurred between 469.86 ±0.62 and 469.63 ±0.60 by U-Pb dating of zircons from the Talacasto
1670 and La Chilca sections of the San Juan Formation, Argentina (Thompson et al., 2012). A second
1671 negative excursion in the early Floian has been recognized globally, and the excursion to positive
1672 values in the later Darriwilian has been identified as the globally recognized MDICE excursion.
1673 Stage slices (SS*) are from Bergstrom et al. (2008) and Time Slices (TS*) are from Webby et al.
1674 (2004).
1675
1676 **Figure 7.** Carbon and sulfur isotope profiles from Argentina. Sulfur isotope compositions were
1677 measured within carbonate-associated sulfate. Average sulfur isotope composition shows a broad
1678 correlation with carbon from the Floian through the Dapingian, followed in the early Darriwilian
1679 by an abrupt shift in the average isotopic composition of marine sulfate. Short-term fluctuations
1680 in the isotopic composition of marine sulfate (cf. Thompson and Kah, 2012) persist through the
1681 entire succession.
1682
1683 **Figure 8.** Carbon and sulfur isotope profiles from western Newfoundland. Sulfur isotope
1684 compositions were measured within carbonate-associated sulfate. As with the Argentine

succession (Fig. 9), An abrupt shift in the average isotopic composition of marine sulfate occurs in the early Darriwilian. Short-term fluctuations in the isotopic composition of marine sulfate persist through the entire succession.

Figure 9. Carbon and sulfur isotope profiles from the Yangtze Platform, South China. Sulfur isotope compositions were measured within carbonate-associated sulfate. Sulfur isotope compositions record a clear correlation with carbon from the Floian through the Dapingian. Short-term fluctuations in the isotopic composition of marine sulfate are not apparent in the deeper-water faices of the succession, suggesting deposition of carbonate beneath a regional chemocline.

Figure 10. Summary of carbon and sulfur isotope profiles from Argentina, Newfoundland, and South China (cf. Figures 7, 8, 9). Similarity in the carbon isotope profile in all three sections is consistent with the existence of a large, well-mixed marine carbon reservoir. Generally heavier carbon isotope values recorded in South China likely reflects proximity to carbon burial. Isotope compositions of CAS show more variability, which is interpreted as reflecting non-conservative behavior in a marine system with low marine sulfate concentrations.

Figure 11. Carbon and sulfur isotope profiles from Argentina and western Newfoundland. Sulfur isotope compositions include both carbonate-associated sulfate and sedimentary pyrite. The mid-Dapingian negative carbon isotope excursion (thin dotted line) correlates to a positive excursion in the isotopic composition of sedimentary pyrite, suggesting enhanced euxinia. An abrupt change in the composition of marine sulfate in the early Darriwilian (heavy dotted line) is

1708 marked by a much slower change in the isotopic composition of marine sulfide. The Darriwilian
1709 is subdivided into Time Slices (Dw1, DW2, Dw3; Webby et al., 2004) and Stage Slices (4a, 4b,
1710 4c; Bergstom et al., 2008), with the time-scale for observed change estimated from Shields et al.
1711 (2003) and modified to reflect most recent geochronological data. Isotopic enrichment of
1712 sedimentary sulfide is interpreted to reflect depletion of hydrogen sulfide within the anoxic
1713 marine reservoir, culminating in the formation of superheavy pyrite (grey band).
1714
1715 **Figure 12.** Dual-reservoir model of sulfur cycling in marine systems. Marine sulfur is divided
1716 into two chemically active reservoirs: sulfate [$SO_4^{=}$] and reduced sulfur [HS^-], which includes all
1717 transient reduced sulfur species. Fluxes and their isotopic compositions include input from
1718 crustal weathering (F_W, δ_W); output via deposition of sedimentary sulfur as gypsum (F_{GYP}, δ_{GYP}),
1719 carbonate-associated sulfate (F_{CAS}, δ_{CAS}), or pyrite (F_{PY}, δ_{PY}); as well as bacterial sulfur
1720 reduction with or without expression of sulfur disproportionation (F_{MSR}, ΔS_1), biological sulfide
1721 oxidation (F_{OX}, ΔS_2), and abiotic sulfide oxidation (F_{OX}, ΔS_3).

Figure 1

Figure 1 - one column

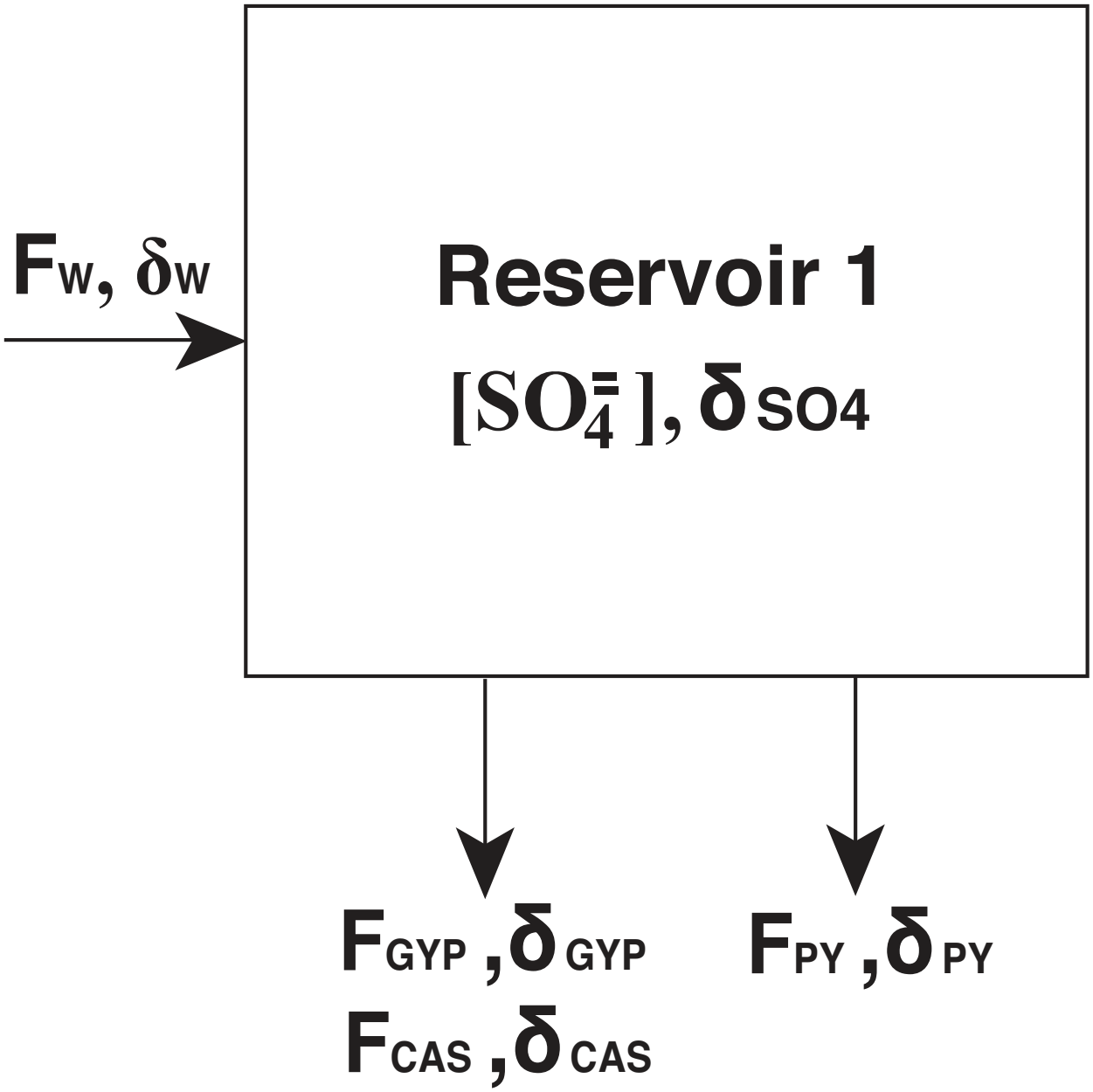

Figure 2

Figure 2 - one column

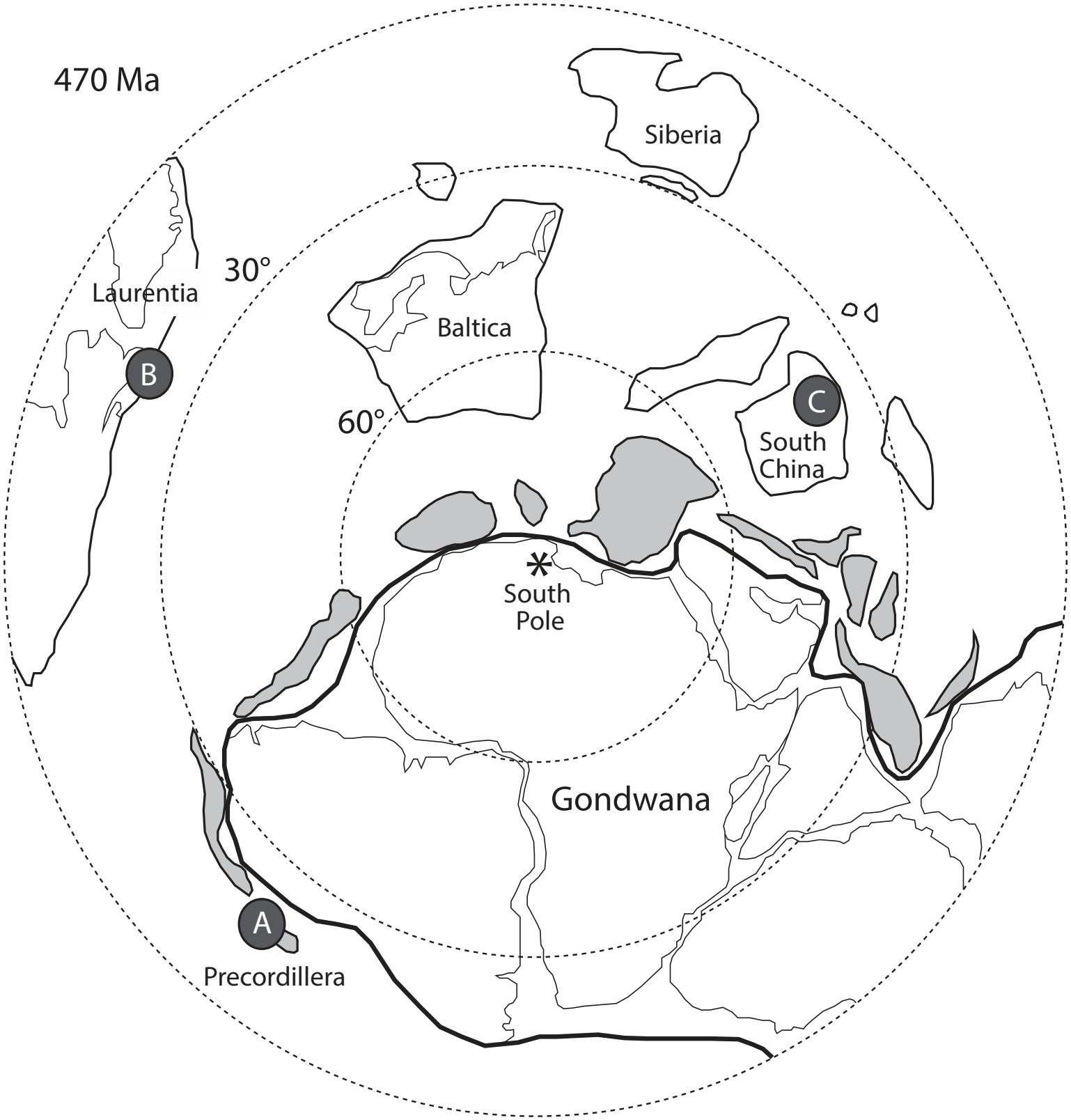

Figure 3

Figure 3 - One Column

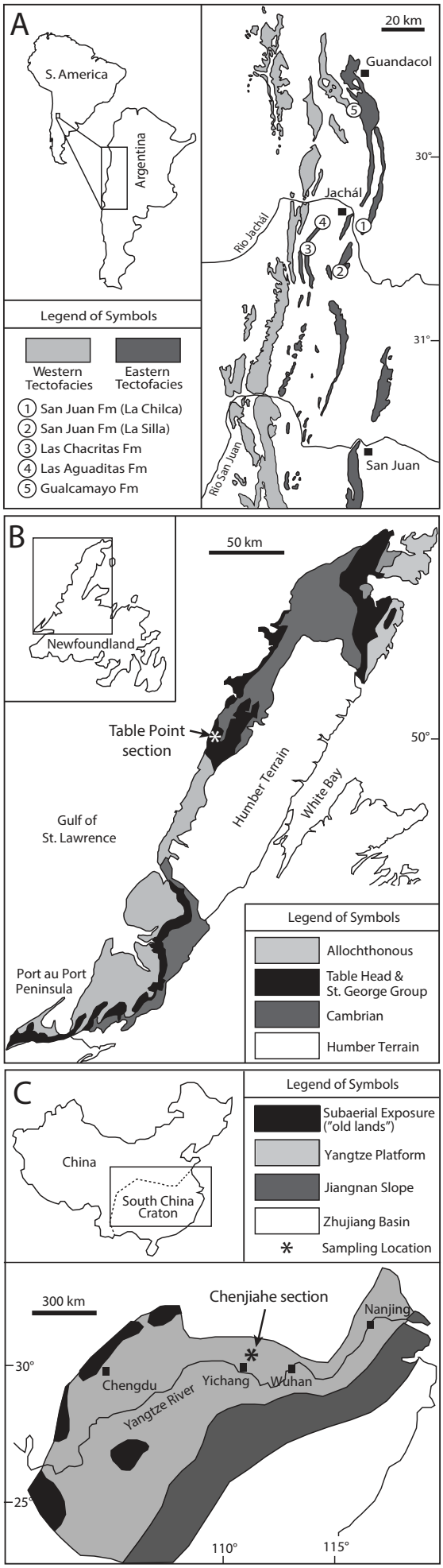

Figure 4

Figure 4 - 2 columns

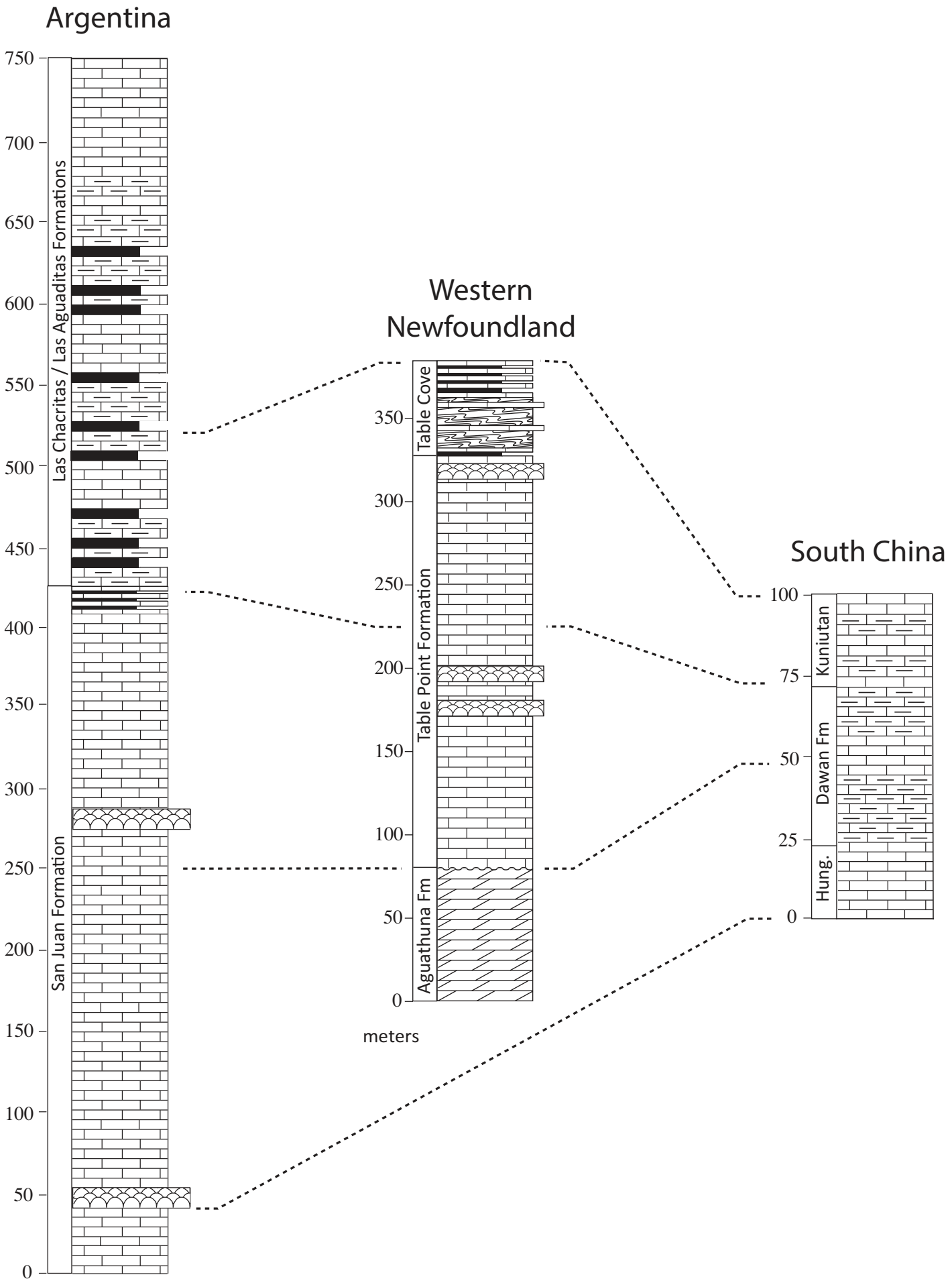

Figure 5

Figure 5 - 2 column

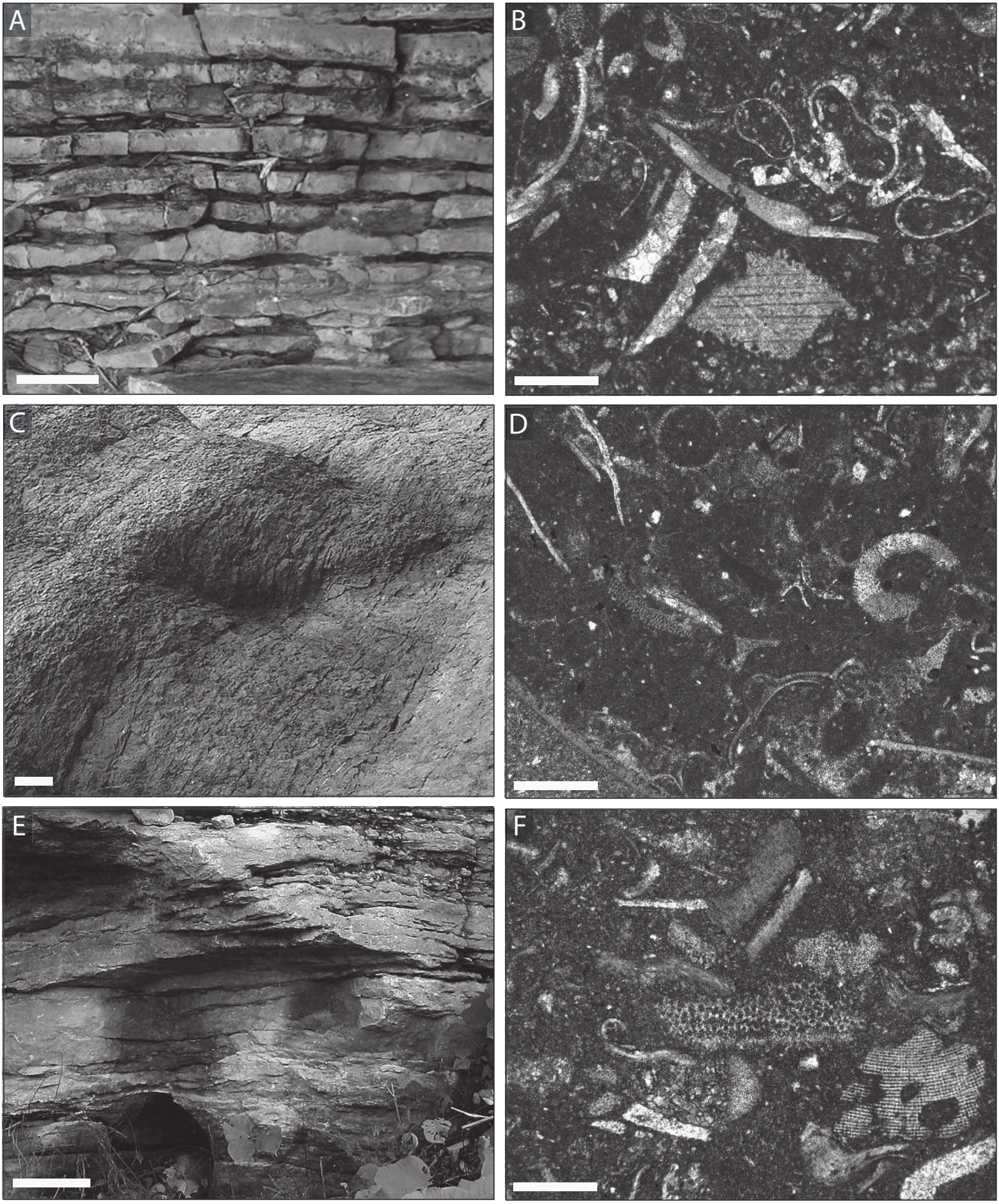

Figure 6

Figure 6 - two columns

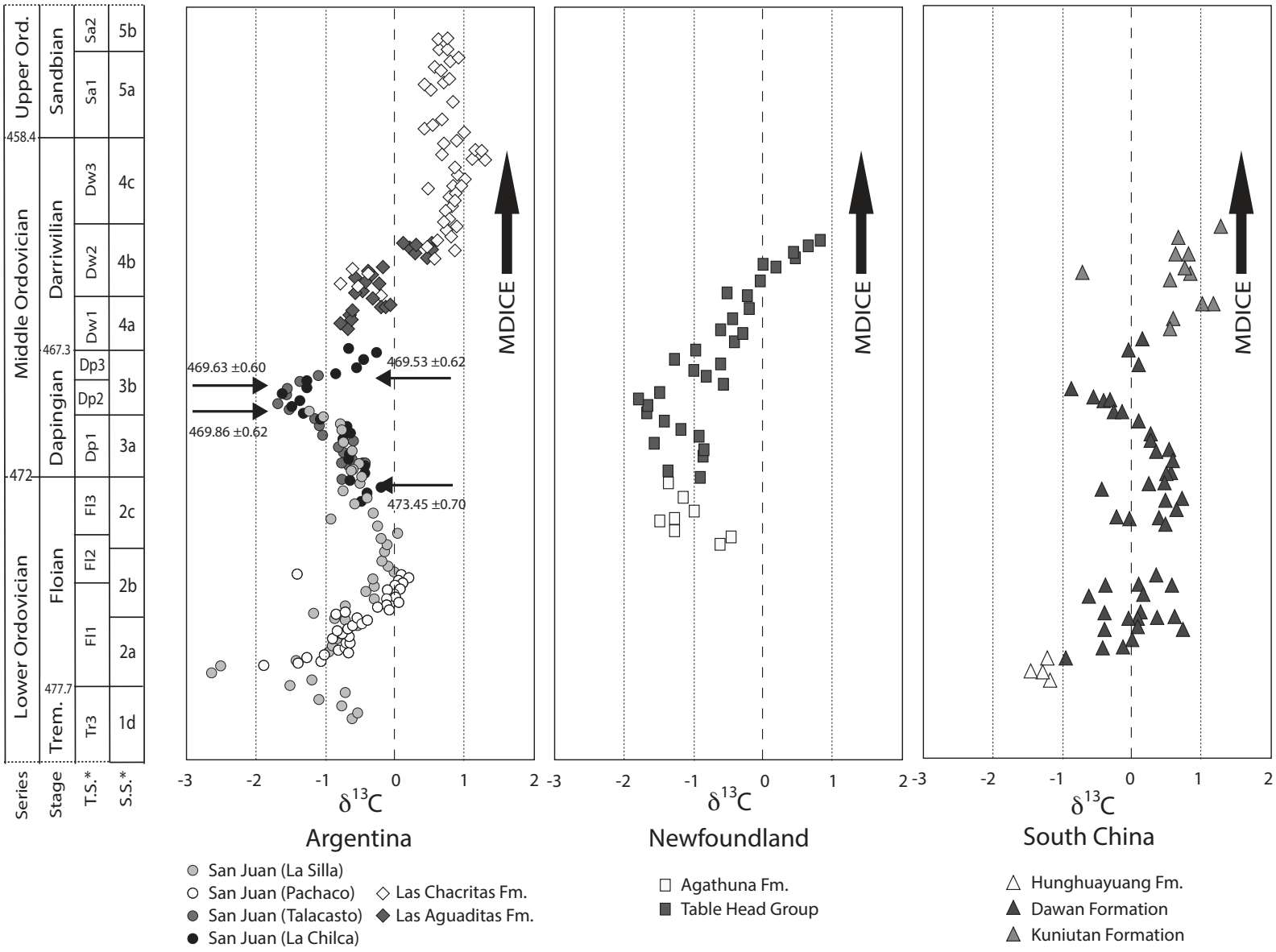

Figure 7

Figure 7 - 2 columns

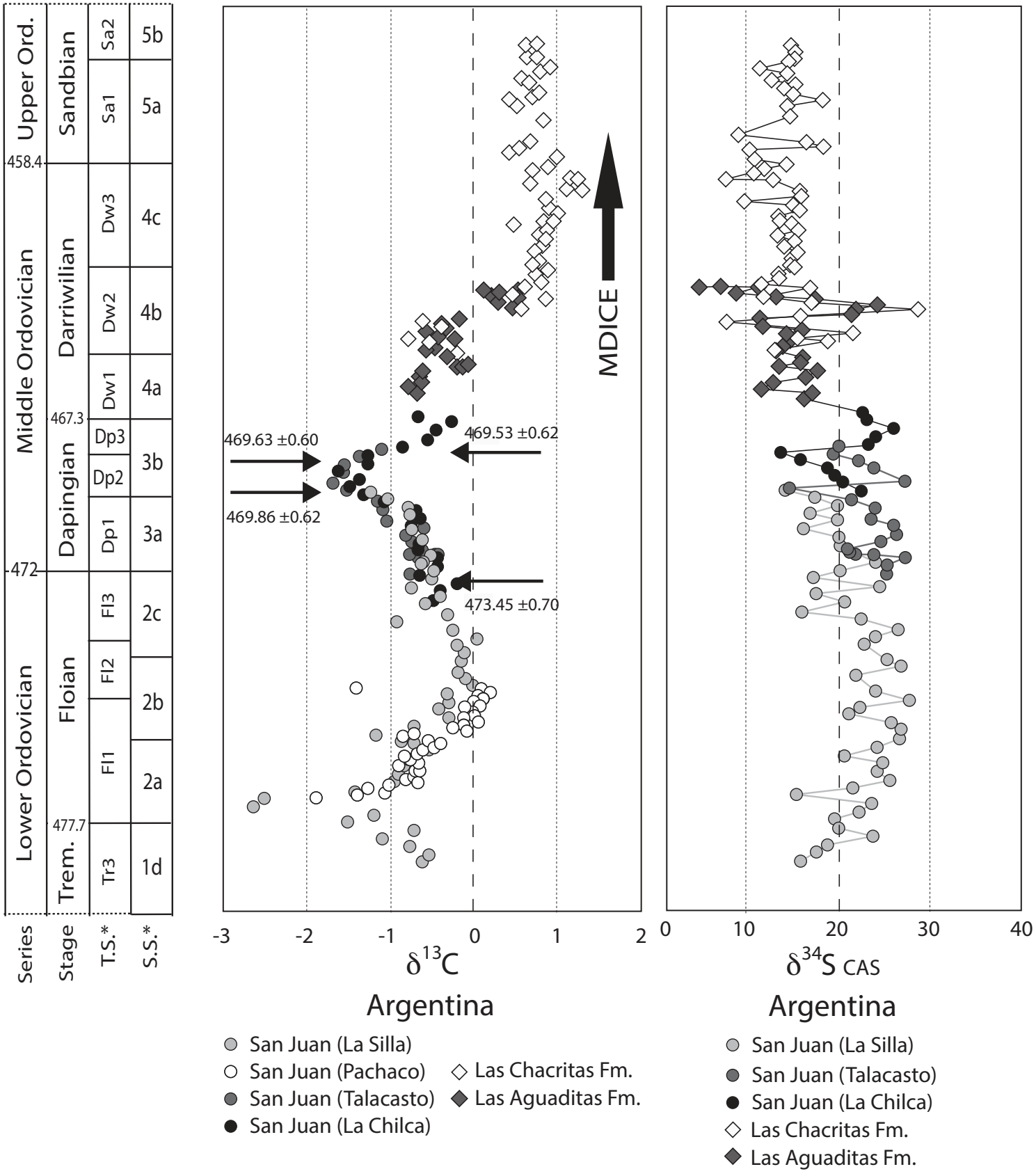

Figure 8

Figure 8 - two columns

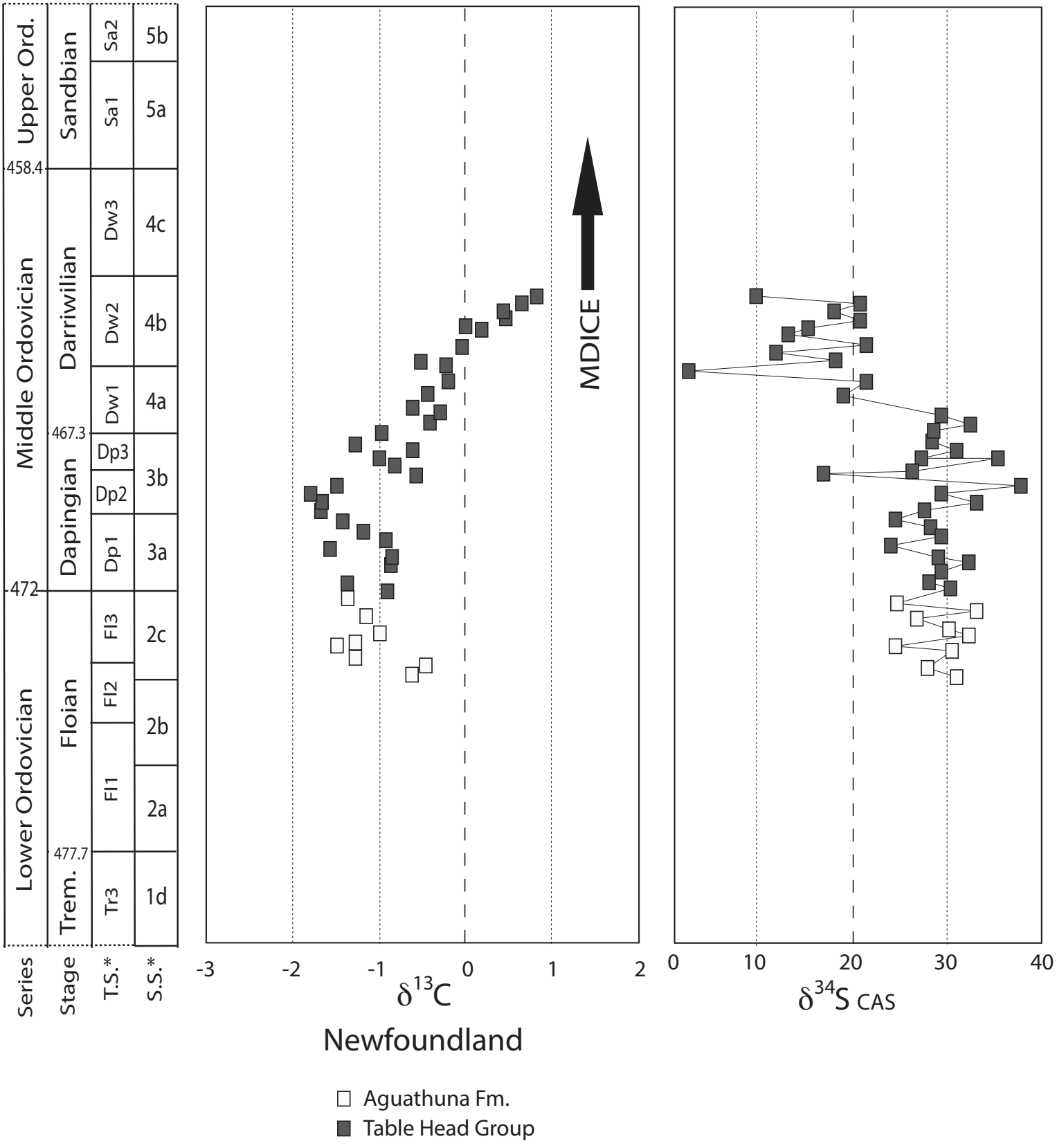

Figure 9

Figure 9 -2 columns

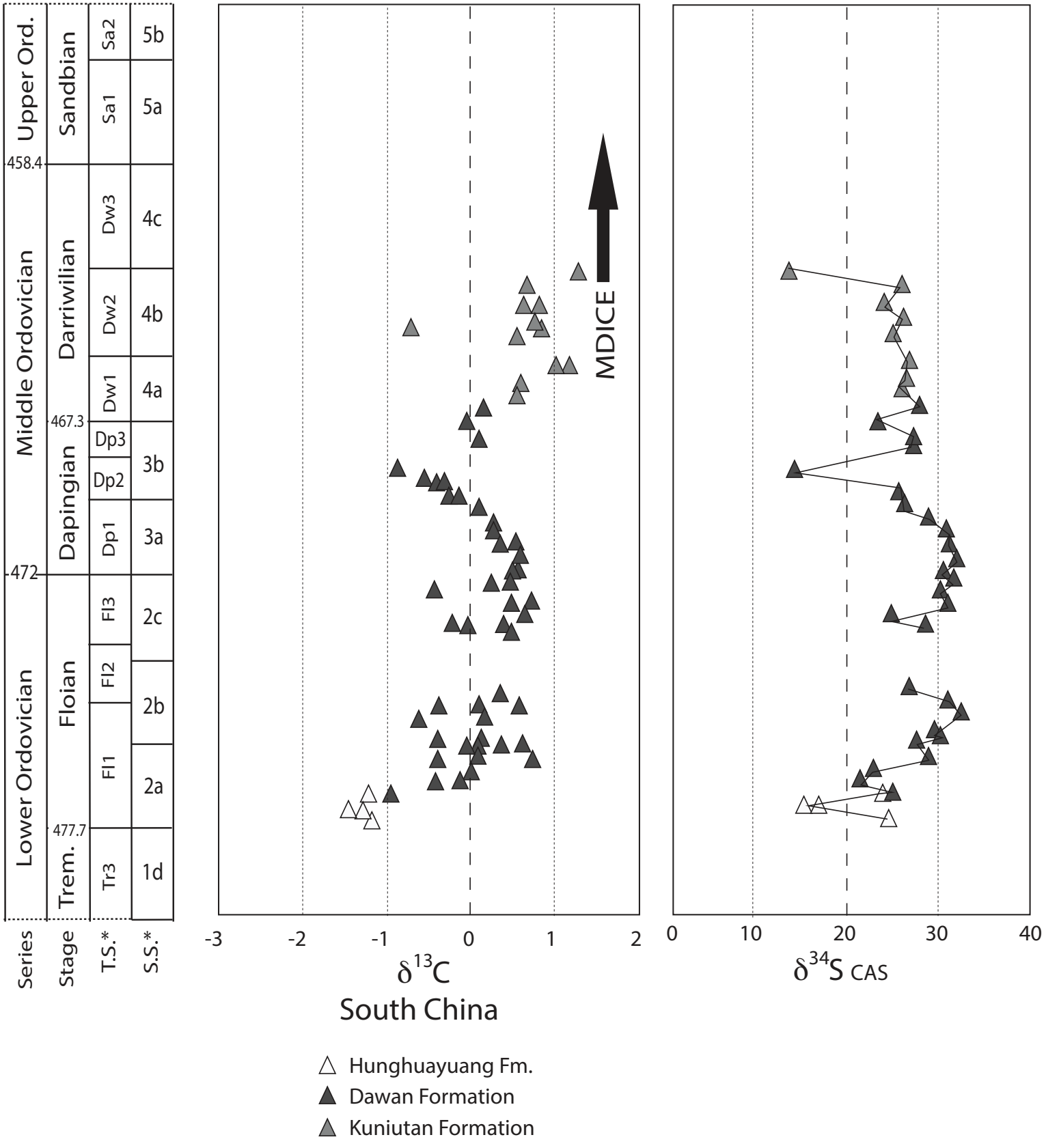

Figure 10

Figure 10 - 2 columns

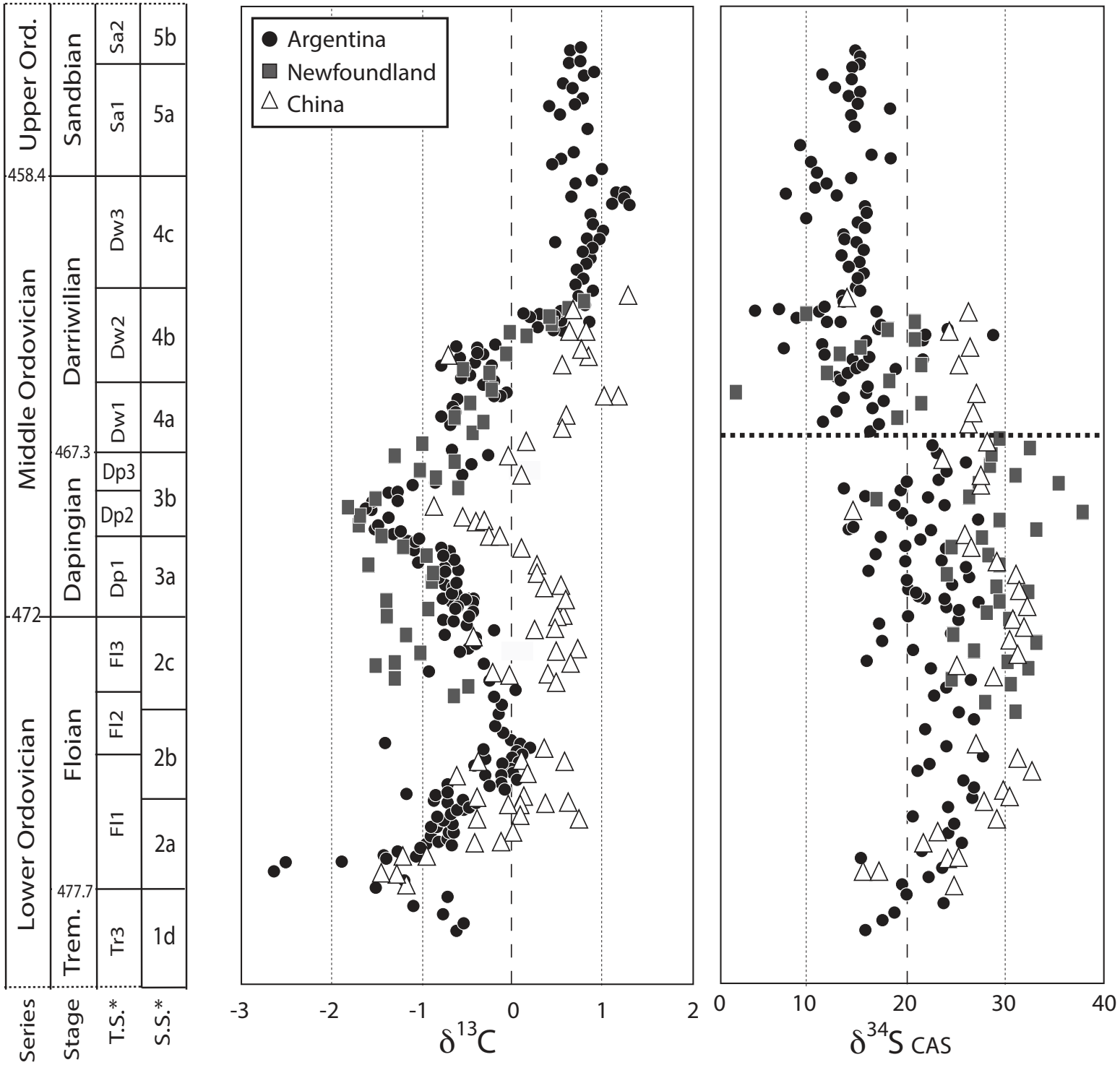

Figure 11

Figure 11 - whole page, turned landscape

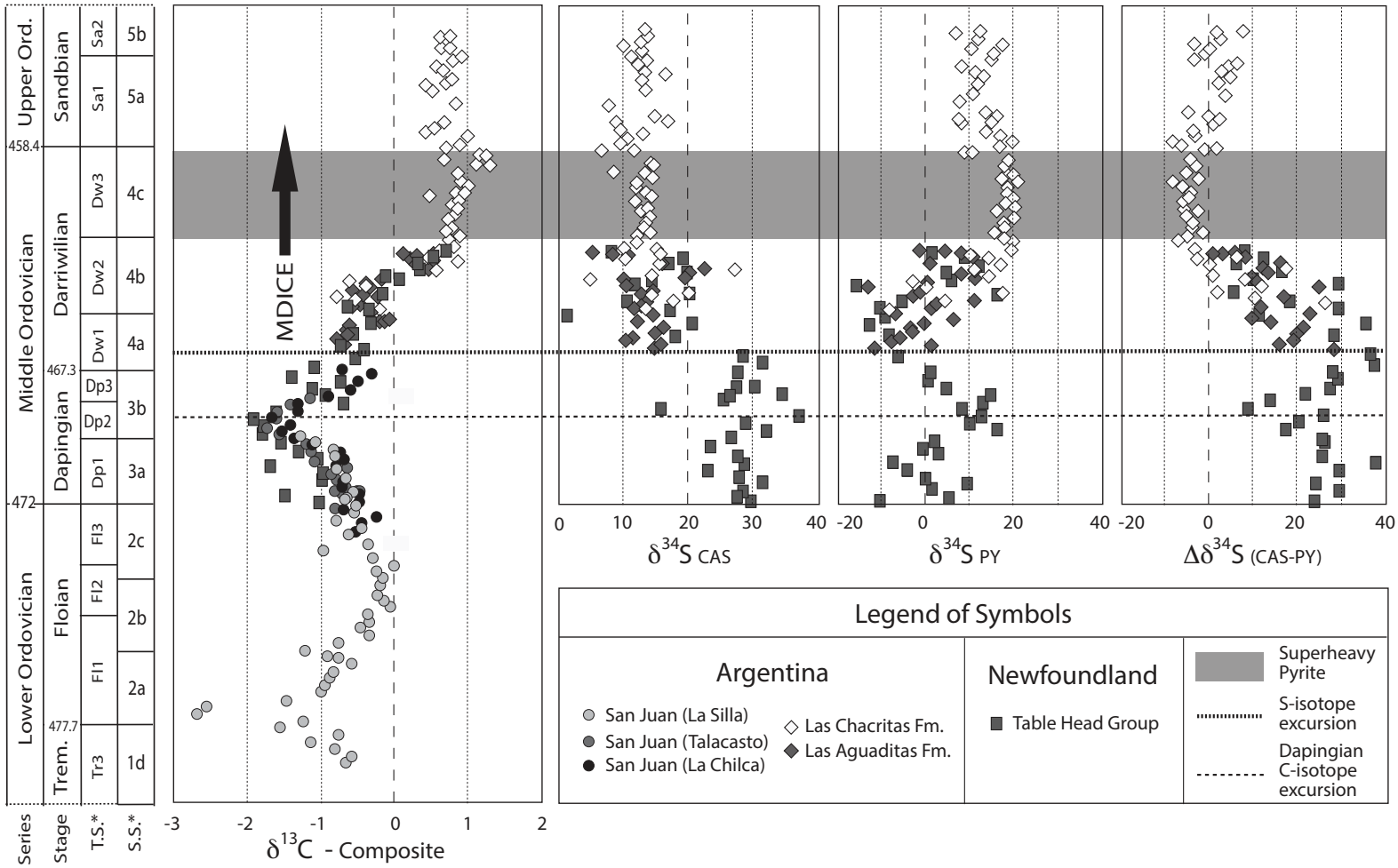

Figure 12

Figure 12 - single column

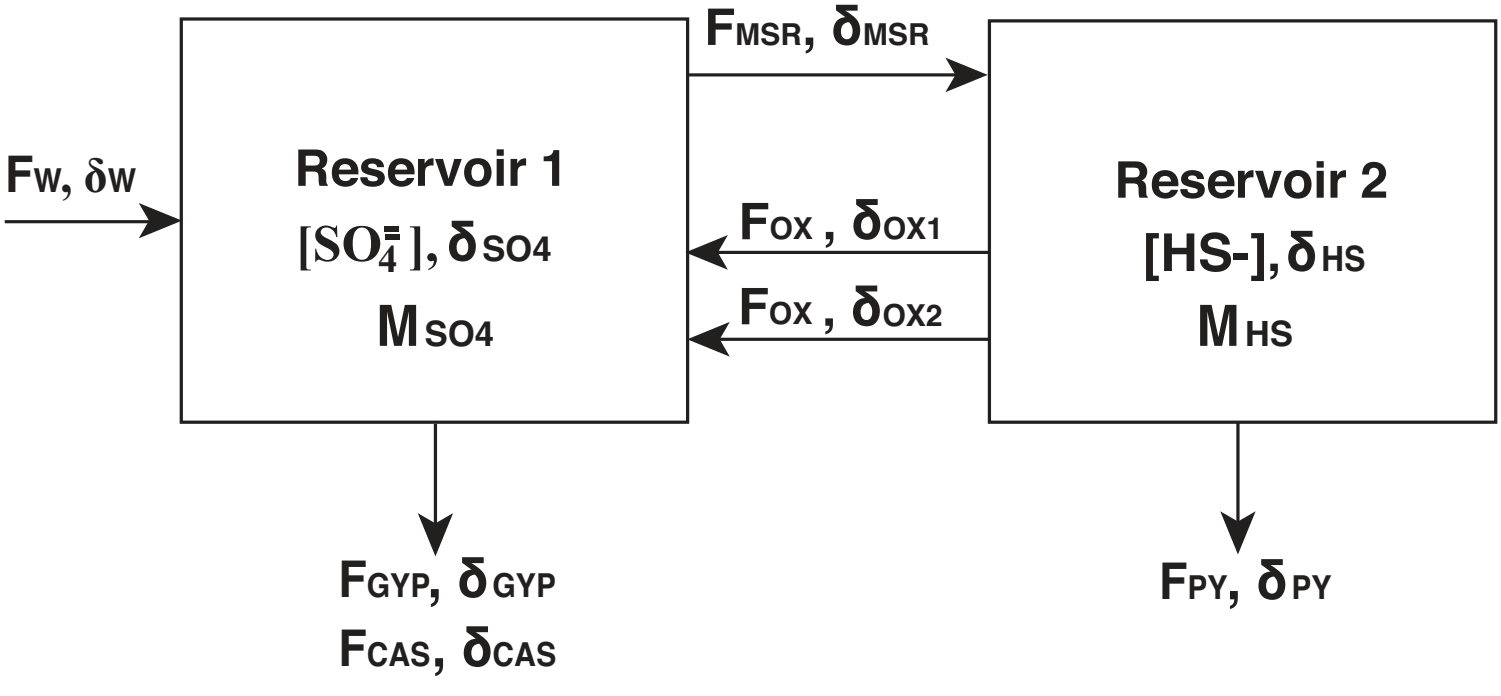

Table 1
Summary of Ordovician isotopic and elemental compositions

	$\delta^{13}C$	$\delta^{18}O$	$\delta^{34}S_{CAS}$	$\delta^{34}S_{PY}$	$\Delta^{34}S$	Mn	Fe	Sr
	‰ (VPDB)		‰ (VCDT)			(PPM)		
San Juan Formation, Argentina								
Average	-0.65	-6.37	21.5	–	–	308	1332	374
St. Dev.	0.46	0.95	3.7	–	–	323	1055	123
Las Chacritas Formation, Argentina								
Average	-0.47	-6.59	14.0	1.4	12.6	515	3346	541
St. Dev.	0.71	0.62	4.5	6.8	7.3	394	3113	244
Las Aguaditas Formation, Argentina								
Average	0.55	-5.19	14.6	14.5	0.1	366	7562	1617
St. Dev.	0.98	0.58	2.3	4.2	4.0	377	8680	610
Aguathuna Formation, western Newfoundland								
Average	-1.22	-9.05	29.6	–	–	–	–	–
St. Dev.	0.37	2.10	3.4	–	–	–	–	–
Table Point and Table Cove formations, western Newfoundland								
Average	-0.82	-7.09	24.9	2.0	22.6	102	1137	513
St. Dev.	0.79	0.45	8.1	8.8	9.6	92	1036	305
Hunghuayuan Formation, South China								
Average	-1.15	-8.01	20.1	–	–	699	435	258
St. Dev.	0.09	0.41	5.1	–	–	73	146	29
Dawan Formation, South China								
Average	-0.03	-6.40	27.9	–	–	2985	3943	384
St. Dev.	0.71	1.17	4.0	–	–	1545	2604	288
Kuniutan Formation, South China								
Average	0.63	-6.77	24.7	–	–	862	3510	270
St. Dev.	0.46	0.93	4.4	–	–	448	1382	33